AGU PUBLICATIONS

JGR

Journal of Geophysical Research: Earth Surface

RESEARCH ARTICLE
10.1002/2015JF003509

Special Section:
Glacier Surging and Ice Streaming

Debris entrainment and landform genesis during tidewater glacier surges

Harold Lovell[1,2,3], Edward J. Fleming[2,4,5], Douglas I. Benn[2,6], Bryn Hubbard[7], Sven Lukas[1], Brice R. Rea[8], Riko Noormets[2], and Anne E. Flink[2]

[1]School of Geography, Queen Mary University of London, London, UK, [2]Department of Geology, University Centre in Svalbard (UNIS), Longyearbyen, Norway, [3]Now at Department of Geography, University of Portsmouth, Portsmouth, UK, [4]School of Geography, Earth and Environmental Sciences, University of Birmingham, Birmingham, UK, [5]Cambridge Arctic Shelf Program, Cambridge University, Cambridge, UK, [6]School of Geography and Geosciences, University of Saint Andrews, Saint Andrews, UK, [7]Department of Geography and Earth Sciences, Aberystwyth University, Aberystwyth, UK, [8]School of Geosciences, University of Aberdeen, Aberdeen, UK

Key Points:
- We investigate basal ice and englacial structures at a surge-type glacier
- The formation of both is linked to tectonic processes during the surge
- Melt-out of englacial structures produces proglacial ridge networks

Correspondence to:
H. Lovell,
harold.lovell@port.ac.uk

Citation:
Lovell, H., E. J. Fleming, D. I. Benn, B. Hubbard, S. Lukas, B. R. Rea, R. Noormets, and A. E. Flink (2015), Debris entrainment and landform genesis during tidewater glacier surges, *J. Geophys. Res. Earth Surf.*, *120*, 1574–1595, doi:10.1002/2015JF003509.

Received 26 FEB 2015
Accepted 21 JUL 2015
Accepted article online 24 JUL 2015
Published online 22 AUG 2015

Abstract The englacial entrainment of basal debris during surges presents an opportunity to investigate processes acting at the glacier bed. The subsequent melt-out of debris-rich englacial structures during the quiescent phase produces geometrical ridge networks on glacier forelands that are diagnostic of surge activity. We investigate the link between debris entrainment and proglacial geomorphology by analyzing basal ice, englacial structures, and ridge networks exposed at the margins of Tunabreen, a tidewater surge-type glacier in Svalbard. The basal ice facies display clear evidence for brittle and ductile tectonic deformation, resulting in overall thickening of the basal ice sequence. The formation of debris-poor dispersed facies ice is the result of strain-induced metamorphism of meteoric ice near the bed. Debris-rich englacial structures display a variety of characteristics and morphologies and are interpreted to represent the incorporation and elevation of subglacial till via the squeezing of till into basal crevasses and hydrofracture exploitation of thrust faults, reoriented crevasse squeezes, and preexisting fractures. These structures are observed to melt-out and form embryonic geometrical ridge networks at the base of a terrestrially grounded ice cliff. Ridge networks are also located at the terrestrial margins of Tunabreen, neighboring Von Postbreen, and in a submarine position within Tempelfjorden. Analysis of network characteristics allows these ridges to be linked to different formational mechanisms of their parent debris-rich englacial structures. This in turn provides an insight into variations in the dominant tectonic stress regimes acting across the glacier during surges.

1. Introduction

Surge-type glaciers erode, entrain, transport, and deposit large volumes of sediment during the active phase of the surge cycle. This material is then exposed during the quiescent phase as characteristic landform-sediment assemblages or surge landsystems [cf., *Evans and Rea*, 1999, 2005]. Sediment is also exposed within the ice as englacial debris inclusions or bands [e.g., *Glasser et al.*, 1998; *Woodward et al.*, 2002], hereafter referred to as debris-rich englacial structures. Better understanding of the links between surging, debris entrainment, and geomorphology is important as it can help to provide an insight into processes acting at the bed [*Christoffersen et al.*, 2005; *Larsen et al.*, 2006]. It also refines the application of surge landsystem models for the interpretation of proglacial geomorphology of glaciers with no known surge history [e.g., *Croot*, 1988; *Ottesen and Dowdeswell*, 2006; *Grant et al.*, 2009] or in paleoenvironments [e.g., *Evans et al.*, 1999; *Lovell et al.*, 2012] and it ensures that glacier-climate inferences are not drawn erroneously from surge moraine systems. Analyzing mechanisms of debris entrainment during surges provides an opportunity to assess this link.

1.1. Debris Entrainment During Glacier Surges

Debris-rich englacial structures have been reported from the margins of a number of surge-type glaciers [e.g., *Gripp*, 1929; *Hambrey and Dowdeswell*, 1997; *Glasser et al.*, 1998; *Lønne*, 2006; *Roberts et al.*, 2009]. These are typically either vertical/near-vertical or dip upglacier when exposed in cross sections parallel to ice flow direction, commonly connect to the bed and can be composed of both sorted and unsorted sediments. It is generally agreed that the structures represent the entrainment and elevation of basal material into the glacier during surges and, in the case of vertical/near-vertical structures, that this is due to squeezing of

soft, deformable till into basal crevasses [e.g., *Rea and Evans*, 2011]. Two main mechanisms have been proposed for the origin of upglacier-dipping structures: (1) debris-bearing thrust faults originating from the bed in a zone of longitudinal compression [e.g., *Hambrey and Dowdeswell*, 1997; *Glasser et al*., 1998; *Lønne*, 2006; *Larsen et al*., 2010] and (2) the deformation of structures initially formed as vertical crevasse squeezes, which are then reoriented in a down-ice direction during quiescent phase ice flow. This forms a favorably inclined slip plane along which thrust-style displacement (TSD) can occur during a subsequent surge [*Evans and Rea*, 1999; *Woodward et al*., 2002; *Rea and Evans*, 2011]. In all cases, formation is related to tectonic processes active during surges and the availability of soft, deformable basal material.

Debris-rich basal ice is sometimes exposed at the margins of surge-type glaciers [e.g., *Sharp et al*., 1994; *Bennett et al*., 2004; *Larsen et al*., 2010]. The properties and character of this debris-rich ice can provide an insight into processes occurring at the glacier bed, particularly in relation to sediment entrainment [e.g., *Lawson*, 1979; *Sugden et al*., 1987; *Alley et al*., 1997], and therefore offer great potential for investigating basal conditions at surge-type glaciers. Numerous ice facies with differing physical characteristics have been described from the base of glaciers and ice sheets [see *Hubbard et al*., 2009]. Of these, debris-rich ice facies are typically thought to have formed due to the entrainment of subglacial material via four main processes: (1) *en masse* freeze-on [e.g., *Weertman*, 1961], (2) regelation around bedrock obstacles [e.g., *Kamb and LaChapelle*, 1964], (3) regelation into the bed [e.g., *Iverson*, 2000], and (4) glacihydraulic supercooling [e.g., *Cook et al*., 2010]. Existing work on basal ice sequences at surge-type glaciers has highlighted the importance of tectonic deformation in their formation, typically resulting in the thickening of units through faulting and folding [*Sharp et al*., 1994; *Larsen et al*., 2010].

When advancing glacier margins encounter preexisting proglacial material, this will either be bulldozed in front, often forming push moraines [e.g., *Boulton et al*., 1999; *Kristensen et al*., 2009], or overridden. In the latter case, the overridden material can be incorporated into the basal sequence through a process known as apron entrainment [cf., *Evans*, 1989]. What is entrained depends entirely upon what is present within the foreland, which can include glacigenic, glacifluvial, and glacilacustrine sediments; buried glacier ice; or proglacial icing deposits [e.g., *Yde et al*., 2005; *Roberts et al*., 2009].

1.2. Geometrical Ridge Networks and Surging

Several surge landsystems have been proposed based on observations at a number of surge-type glaciers [e.g., *Evans and Rea*, 1999; *Ottesen and Dowdeswell*, 2006; *Roberts et al*., 2009; *Brynjólfsson et al*., 2012]. A great deal of variation is apparent, but common landforms identified in most examples are push/thrust-block moraines, glacial lineations, geometrical ridge networks, hummocky moraine, and eskers (both zigzag and sinuous). As with any landsystem, it is the suite of landforms that is diagnostic of surge activity, rather than individual elements in isolation, most of which are found in a large variety of glacial environments. However, geometrical ridge networks are typically only found in relation to surge activity and are preserved on the deglaciated forelands of both terrestrial and tidewater surge-type glaciers [e.g., *Gripp*, 1929; *Sharp*, 1985; *Solheim and Pfirman*, 1985; *Bennett et al*., 1996; *Boulton et al*., 1996; *Ottesen and Dowdeswell*, 2006; *Kjær et al*., 2008; *Ottesen et al*., 2008; *Kristensen et al*., 2009; *Rea and Evans*, 2011; *Flink et al*., 2015]. Geometrical ridge networks comprise individual ridges that are generally sharp crested, composed of diamict, may be aligned parallel, transverse, or oblique to dominant ice flow direction, and are typically ~1–3 m high, $<$2 m wide and tens of meters long. The ridges are commonly arranged in interconnected networks with a distinct rhombohedral or rectilinear pattern, whereby two principal orientations dominate, often forming conjugate pairs offset slightly from an alignment transverse to ice flow. In most cases, geometrical ridge networks are interpreted as melted-out crevasse squeezes entrained during the active phase, before being exposed as ice stagnates and recedes during the quiescent phase [e.g., *Gripp*, 1929; *Sharp*, 1985; *Boulton et al*., 1996; *Evans and Rea*, 1999; *Ottesen and Dowdeswell*, 2006; *Flink et al*., 2015]. Alternative interpretations suggest that ridge networks can also be derived from debris-bearing thrust faults [e.g., *Bennett et al*., 1996; *Glasser et al*., 1998]. Either way, they have been strongly linked to the unique conditions of englacial debris entrainment during surges followed by stagnation, but direct observations of this connection are typically absent. Investigation of the links between surge phase processes, mechanisms of debris entrainment, and the subsequent formation of geometrical ridge networks can therefore provide further insight into the geomorphological record produced by episodic rapid ice flow followed by widespread stagnation. This may also be relevant to understanding paleo–ice stream dynamics [e.g., *Klages et al*., 2013; *Andreassen et al*., 2014].

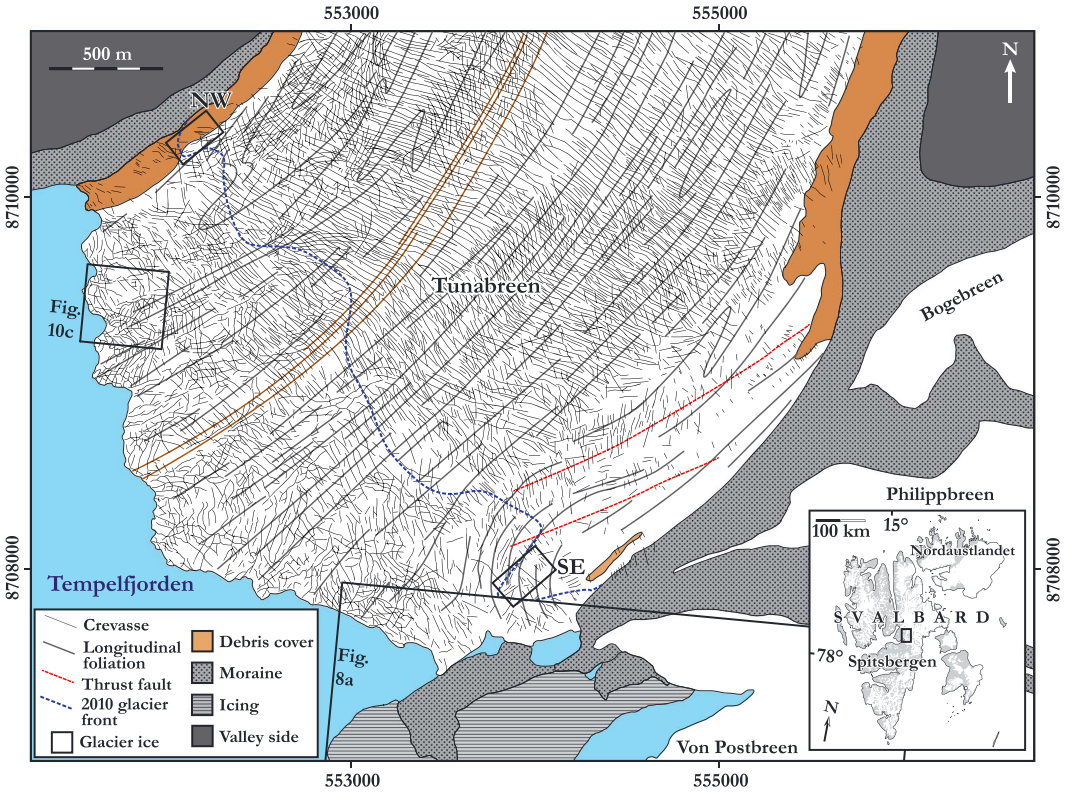

Figure 1. Glaciological structural map of Tunabreen at its most recent surge maximum in August 2004. Blue dashed line shows position of glacier front in 2010. Locations of NW and SE sections are shown in relation to both the 2004 and the 2010 positions. Inset shows location of study area within Svalbard.

1.3. Research Aims

This study investigates debris entrainment and landforming processes which occurred during surges of Tunabreen, a tidewater glacier in Svalbard by (1) characterizing and determining the origin of debris-rich basal ice exposed at the glacier's lateral margins, (2) assessing the formation of debris-rich englacial structures and their possible links to surge processes, and (3) examining the connection between debris-rich englacial structures and the formation of proglacial geometrical ridge networks. We build on work at this site by *Fleming et al*. [2013], who used anisotropic magnetic susceptibility (AMS) to derive fabric data from the basal ice and linked this to surge ice flow dynamics.

2. Study Area

Tunabreen drains the Lomonosovfonna and Filchnerfonna ice caps and terminates at the head of Tempelfjorden (78°26'N, 17°19'E; Figure 1). The glacier is ~33 km long and is ~3 km wide for much of its length, including at its tidewater margin, where it terminates as a ~40 m high ice cliff grounded in water of approximately the same depth [*Flink et al*., 2015]. Tunabreen is unique in terms of Svalbard surging glaciers because it has been observed to surge three times (1930s, 1971, and 2003–2005), with a consistent return period of ~40 years [*Flink et al*., 2015]. Neighboring Von Postbreen last surged toward the end of the Little Ice Age (LIA) circa 1870, since when it has undergone sustained retreat and transitioned from a tidewater front to a land-terminating glacier. Terminus fluctuations in Tempelfjorden since the LIA, encompassing the surges of Tunabreen, are described in *Flink et al*. [2015].

The most recent surge began between June 2002 and July 2003 and reached a maximum position at, or soon after, July 2004 following an advance of ~2 km. The front has receded ~1.5 km since surge termination. During this period two large calving bays developed in the front, leaving a notable peninsula at the SE margin within which sections SE-A and SE-B (Figure 1) are located.

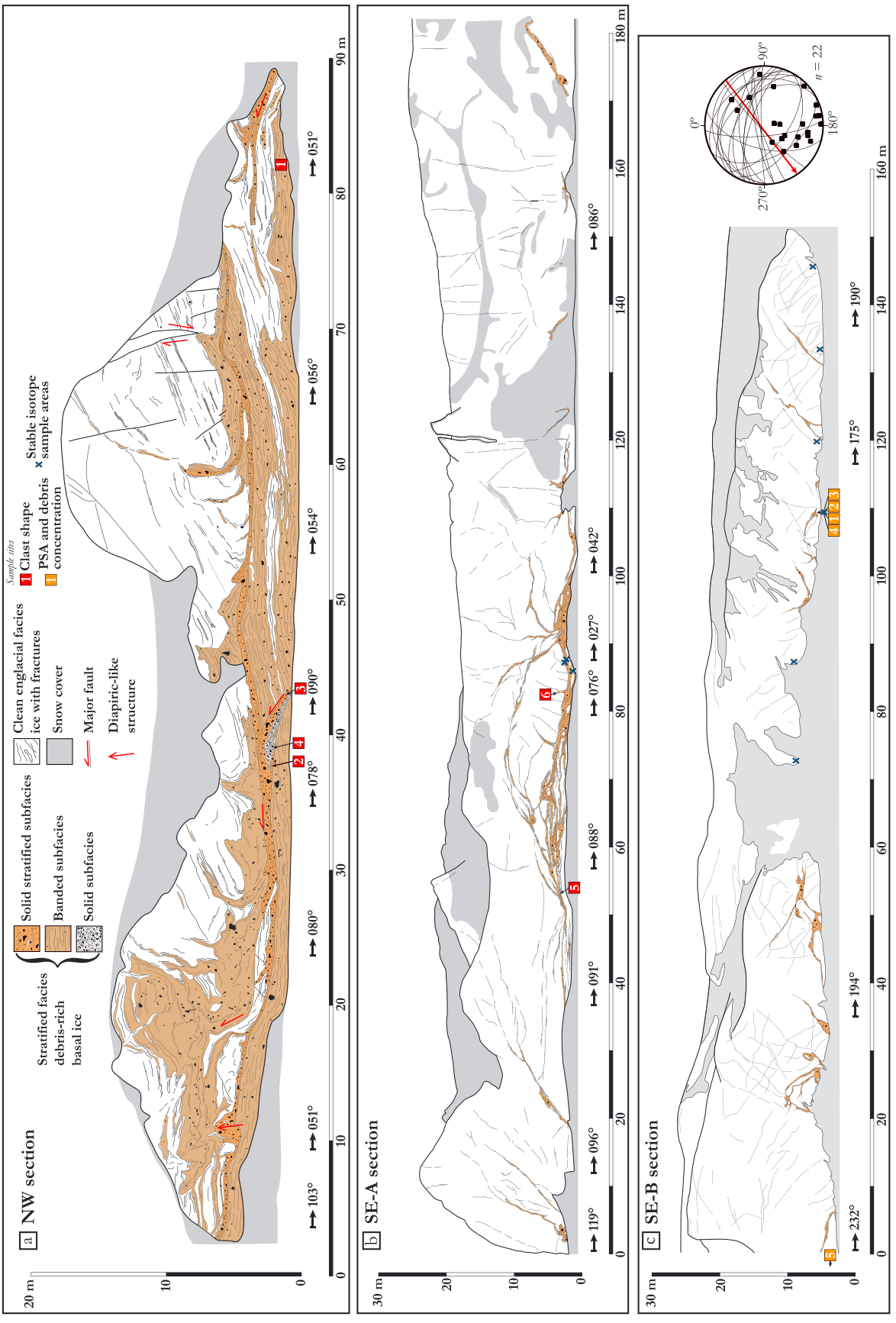

Figure 2. Two-dimensional section logs. (a) NW section. (b) SE-A section. (c) SE-B section. Orientations of some debris-rich englacial structures within SE-B are plotted onto a lower hemisphere, equal-area stereographic projection. Red arrows on stereograph shows centerline ice flow direction at the terminus.

Table 1. Key Characteristics of Ice Facies Identified at Tunabreen

Ice Facies	Thickness (m)	Physical Characteristics	Proposed Origin
Englacial (En)	>10	White, opaque appearance; bubble rich; contains alternations of bubble-rich and bubble-poor ice; and very low debris content	Meteoric ice
Dispersed (D)	~0.1–1.5	Variable bubble content, ranging from clear, bubble-free ice to dense, white clouds of bubbles and intercalated bubble-rich and bubble-poor layers; low debris content (<1%), largely consisting of suspended grains, clots, or thin laminae of silt-sized material	Strain-induced metamorphism of englacial facies
Stratified			
Solid stratified (Ss)	~0.1–2.5	Debris-rich, consisting of poorly sorted diamict; estimated debris content ranges from ~50 to 75%; contains bubble-free clear ice lenses and interstitial ice	Basal freeze-on of saturated subglacial debris
Banded (Bd)	~0.1–15	Alternations of laterally discontinuous debris-rich and debris-poor laminae, typically aligned subhorizontally in relation to the section base; debris ranges from individual grains or clots of silt up to poorly sorted diamict; typical debris content ranges from ~10 to 30%	Tectonic thickening of laminated debris-rich/clean ice originally entrained through freeze-on and regelation
Solid (S)	~0.2–1	Frozen, structureless diamict with interstitial ice clast-supported in places and composed almost entirely of angular limestone clasts	Freeze-on of rockfall/little-modified material

3. Methods

Distributions of ice facies and debris-rich structures exposed within terrestrially grounded ice cliffs at the NW and SE margins of Tunabreen were recorded as two-dimensional logs (Figure 2; see *Fleming et al.* [2013] for section photographs). Ice facies classification was based on physical characteristics following *Hubbard et al.* [2009], including overall facies thickness, structure, debris concentration, and bubble content (Table 1). Decimeter-scale blocks were sampled for debris concentration, grain size distribution, and stable isotope analysis. Debris concentrations (percent by volume) were calculated following the methods outlined in *Knight* [1997] and *Waller* [1997], whereby samples were melted in a beaker, debris was allowed to settle, and the total volume and the volume of the debris were recorded. Grain size distributions were determined by dry sieving (-4.0 to $0.5\,\varphi$) and laser granulometry ($>0.5\,\varphi$). Particle size distributions derived from laser granulometry (percent by volume) were calculated as a percentage of the entire sample weight and were plotted together with the distributions derived from sieving (percent by weight) after standardization. Samples for clast shape analysis were collected according to *Lukas et al.* [2013]. Sheared englacial debris laminae and planar debris-rich structures were recorded in three dimensions using a compass-clinometer and plotted as equal-area stereographic projections. Samples for stable isotope analysis [e.g., *Souchez and Jouzel*, 1984; *Souchez et al.*, 1988] were either extracted directly using an ice screw or filtered from melted ice blocks. All samples were stored in 30 mL high-density polyethylene narrow-neck, screw-top bottles and analysis was undertaken at the University of Birmingham, UK, on a GV Instruments Isoprime continuous-flow mass spectrometer. Statistical comparisons of the isotope data between different facies are reported at the 95% confidence level (i.e., ±2 standard deviations). The bathymetric data were acquired by the Norwegian Hydrographic Service with a Kongsberg EM3002 300 kHz multibeam echosounder system.

4. Results

4.1. Ice Facies

4.1.1. Englacial Facies (En)

This is the dominant facies within the glacier and consists of clean (debris-poor) ice with a high bubble content, giving it an opaque, bluish-white appearance. In places this facies is stratified at centimeter to decimeter scales in the form of intercalated layers of bubble-rich and bubble-poor ice (Table 1 and Figure 3a). Apart from some ~0.5–2 m thick layers and isolated lenses/blocks within the stratified facies (Figure 2a), englacial facies ice typically overlies the dispersed and debris-rich stratified facies. Stable isotope analysis of englacial facies ice ($n = 6$) yielded mean compositions of -15.34‰ and -100.83‰ for δ^{18}O and δD, respectively (Table 2 and Figure 4).

4.1.2. Dispersed Facies (D)

This facies is composed primarily of clean ice with typically very low debris content (Figures 3b and 3c), visually estimated at <1%, and is largely devoid of internal stratification (Table 1). The debris consists

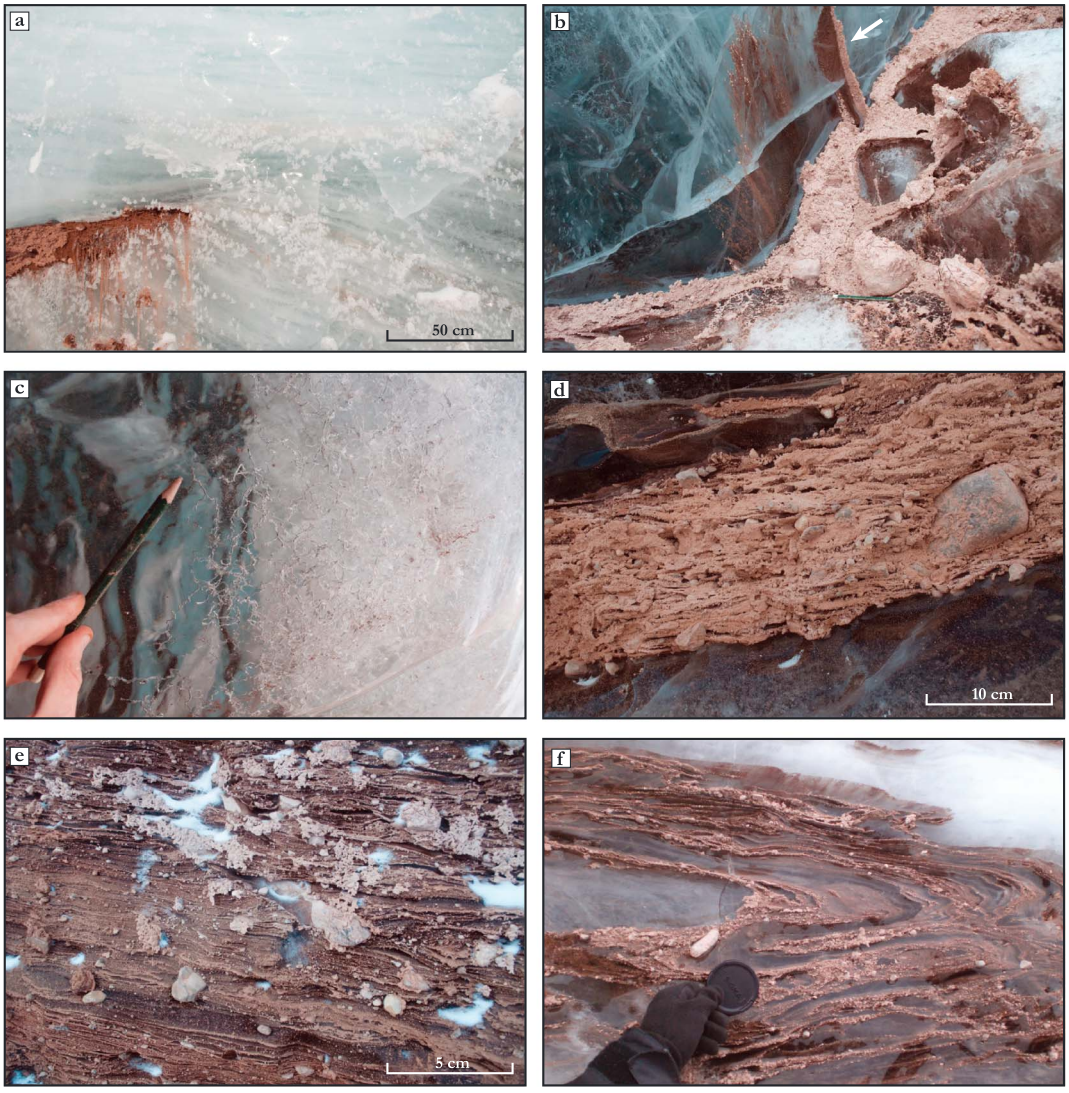

Figure 3. Examples of ice facies. (a) Englacial facies ice surrounding a debris band, SE-A section. (b) Debris laminae (arrowed) within dispersed facies ice extending from debris-rich structure, SE-A section. (c) Thin filament-like bubble structures within dispersed facies ice, SE-A section. (d) Solid stratified subfacies, NW section. Note the stratification picked-out by thin ice lenses. (e) Banded subfacies, NW section. (f) Isoclinal Z-shaped fold verging to right within banded subfacies, SE-A section.

predominantly of isolated grains or small clots and very thin (<5 mm) laminae (Figures 3b and 5c). The bubble content ranges from no or very few bubbles, where the ice is clear and translucent, up to bubble-rich ice with a white, opaque appearance, which often grades indistinguishably into the overlying englacial facies. The clearest, bubble-free areas of this facies are almost always in contact with debris-rich stratified ice (Figure 3b) and in places contain discrete linear filaments of very fine bubbles (<1 mm; Figure 3c). The individual strands of these structures are only one bubble thick and typically extend away from

Table 2. Summary of Isotope Data[a]

Ice Facies	*n*	Section	δ^{18}O Mean (‰), Standard Deviation and Range	Enriched	δD Mean (‰), Standard Deviation and Range	Enriched
All samples	32	All	−14.36 ± 0.98 (−12.99 to −16.50)	-	−102.75 ± 6.78 (−86.51 to −118.22)	-
Englacial	6	SE-A, SE-B	−15.34 ± 0.68 (−14.62 to −16.13)	-	−100.83 ± 7.16 (−86.51 to −105.40)	-
Dispersed	20	SE-A, SE-B	−14.20 ± 1.02 (−12.99 to −16.50)	No	−103.12 ± 7.18 (−94.40 to −118.22)	No
Stratified	6	SE-B	−13.94 ± 0.25 (−13.57 to −14.31)	Yes	−103.41 ± 5.69 (−94.40 to −110.45)	No

[a]"Enriched" indicates whether ice facies were enriched in heavy isotopes relative to mean values of δ^{18}O and δD for the englacial facies at the 95% confidence level (i.e., ± 2 standard deviations).

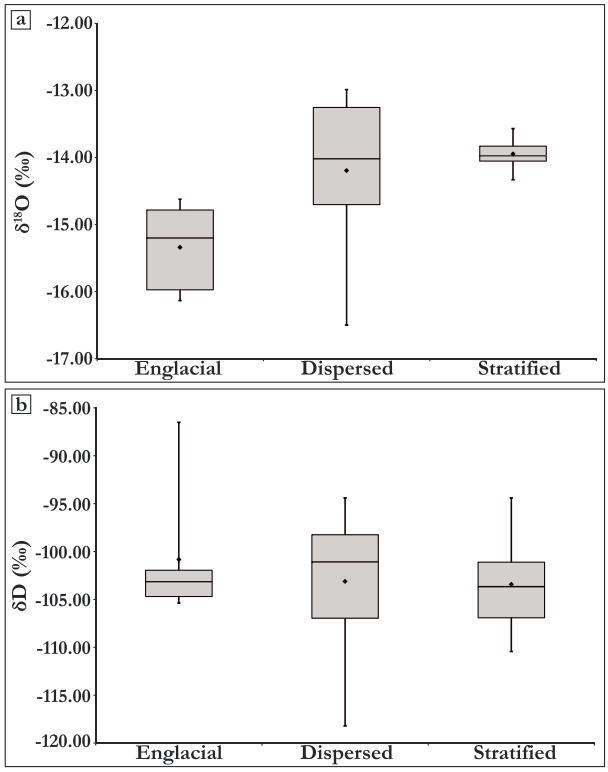

Figure 4. Box plots of stable isotope analysis of ice facies showing maximum, upper quartile, median, mean (black diamond), lower quartile, and minimum values. (a) δ^{18}O composition and (b) δD composition.

debris-rich ice. Some of the bubble structures contain fine-grained debris. In places, a gradation can be seen from filaments into wider (~1–10 mm) linear, ribbon-like bubble structures with a planar form. These bubble structures appear to follow the boundaries of large (centimeter-scale) ice crystals.

Stable isotope analysis (Table 2 and Figure 4) returned mean values for the dispersed facies ($n = 20$) of −14.20‰ (δ^{18}O) and −103.12‰ (δD). The dispersed facies samples are not statistically distinguishable from the englacial facies at the 95% confidence level. No linear relationships (e.g., freezing slopes) are found when the data are plotted coisotopically.

4.1.3. Stratified Facies

The stratified facies is debris-rich and has been subdivided into three subfacies: solid stratified, banded, and solid (Table 1). In places, especially at the SE sections, the differentiation between the solid stratified and banded subfacies is indistinct and they appear to exist on a continuum. Stratified facies ice is the dominant facies at the NW section and within the debris-rich structures exposed at the SE sections (Figure 2).

4.1.3.1. Solid Stratified Subfacies (Ss)

The solid stratified subfacies is composed of frozen diamict with interstitial ice and small lenses of clean ice with no or very few bubbles (Figure 3d). The diamict is matrix supported and has a polymodal grain size distribution (Figure 5c), including occasional boulders up to 0.5 m in diameter. Clasts are typically subangular to subrounded (Figure 5a) and striated. The solid stratified subfacies is in general crudely stratified, highlighted by the presence of numerous thin clean ice lenses (Figure 3d), but in some areas can also appear structureless. The debris content of the stratified facies is variable and ranges from measured values of 9.6–52.0% (by volume) at the SE-B section (Figure 2c). Visual estimates suggest higher concentrations of ~75% are typical.

4.1.3.2. Banded Subfacies (Bd)

The banded subfacies is characterized by laterally discontinuous debris-rich laminae separated by layers of clean ice containing no or very few bubbles (Figures 3e and 3f). The thickness of the debris-rich laminae ranges from <1 to 30 mm and the spacing between ranges from ~1 to 40 mm. The debris size ranges from individual grains or clots of silt and sand within the thinner laminae up to diamict (Figures 3e, 5a, and 5c). This subfacies generally has lower debris concentrations than the solid stratified subfacies, and the measured debris contents of 9.6% and 31% for stratified facies ice were selected to reflect the two endmembers of relatively debris-poor (Figure 3f) and debris-rich (Figure 3e) ice within this subfacies.

4.1.3.3. Solid Subfacies (S)

The solid subfacies is a frozen, massive, and matrix-supported diamict, consisting of predominantly angular limestone clasts (Figure 5a), and is only observed at the NW section (Figure 2a).

4.1.3.4. Stable Isotope Analysis

Stable isotope analysis (Table 2 and Figure 4) returned mean values for the stratified facies ($n = 6$) at the SE-B section (Figure 2c) of −13.94‰ (δ^{18}O) and −103.41‰ (δD). These results show that the stratified facies is heavier than mean values of the englacial facies and this difference is statistically significant. No statistically significant linear relationship (e.g., freezing slopes) is apparent when the data are plotted coisotopically.

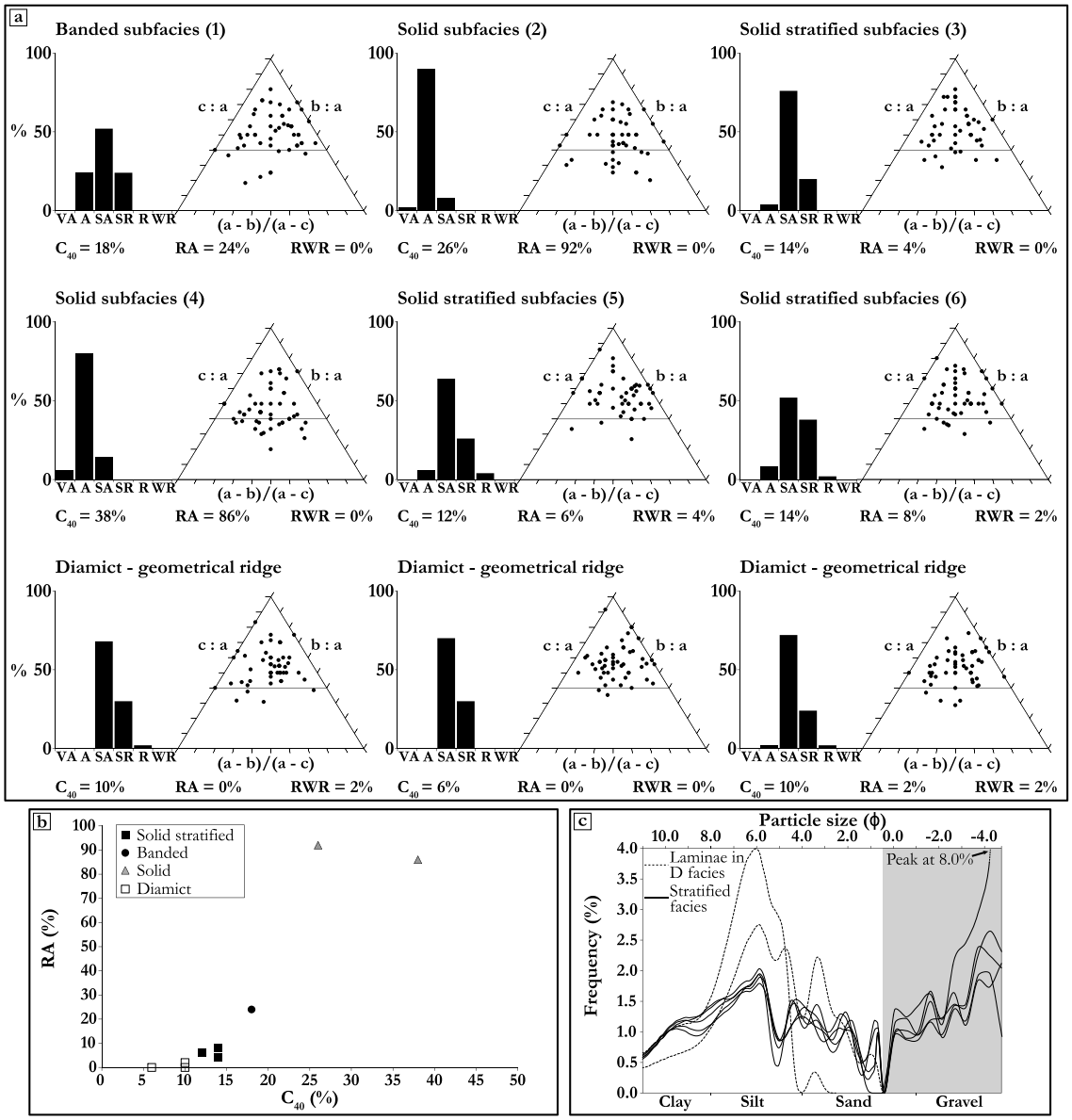

Figure 5. Sedimentary characteristics of stratified and dispersed ice facies and diamict within geometrical ridges. (a) Clast shape data from stratified facies and diamict within geometrical ridges plotted on histograms (roundness) and ternary diagrams (shape). Each sample is of 50 sandstone clasts. Numbers in brackets refer to sample numbers in Figure 2. (b) RA-C_{40} diagram for clast shape data. (c) Grain size distributions of stratified facies (solid blue line; $n = 5$) and debris laminae within dispersed facies (dashed red line; $n = 2$) from SE-B section. Sample locations shown on Figure 2c. Troughs in the data are likely to be an artefact of combining dry sieving and laser granulometry methods.

4.2. Ice Facies Stratigraphy and Debris-Rich Englacial Structures

4.2.1. NW Section

This section is characterized by thick (up to 10 m) sequences of stratified facies ice intercalated with thinner (up to 2 m) layers of clean englacial and dispersed facies ice (Figure 2a). The majority of the section is composed of banded subfacies ice, typically aligned parallel to subparallel to the base of the section (Figures 2a and 6a). Toward the left-hand (SW) end, the lamination is often folded, including a close, inclined, asymmetric z-shaped fold at ~70 m along section (as) (Figure 6b). This example is closely associated with both a large-scale slightly inclined open fold of the underlying solid stratified layer and a normal fault (vertical displacement ~70 cm) within the englacial facies above (Figure 6b).

The solid stratified subfacies forms a near-continuous layer at the NW section, typically 0.5 m thick and up to a maximum thickness of 2.5 m at ~11 m (as) (Figures 2a and 6a–6d). This layer overlies banded subfacies ice

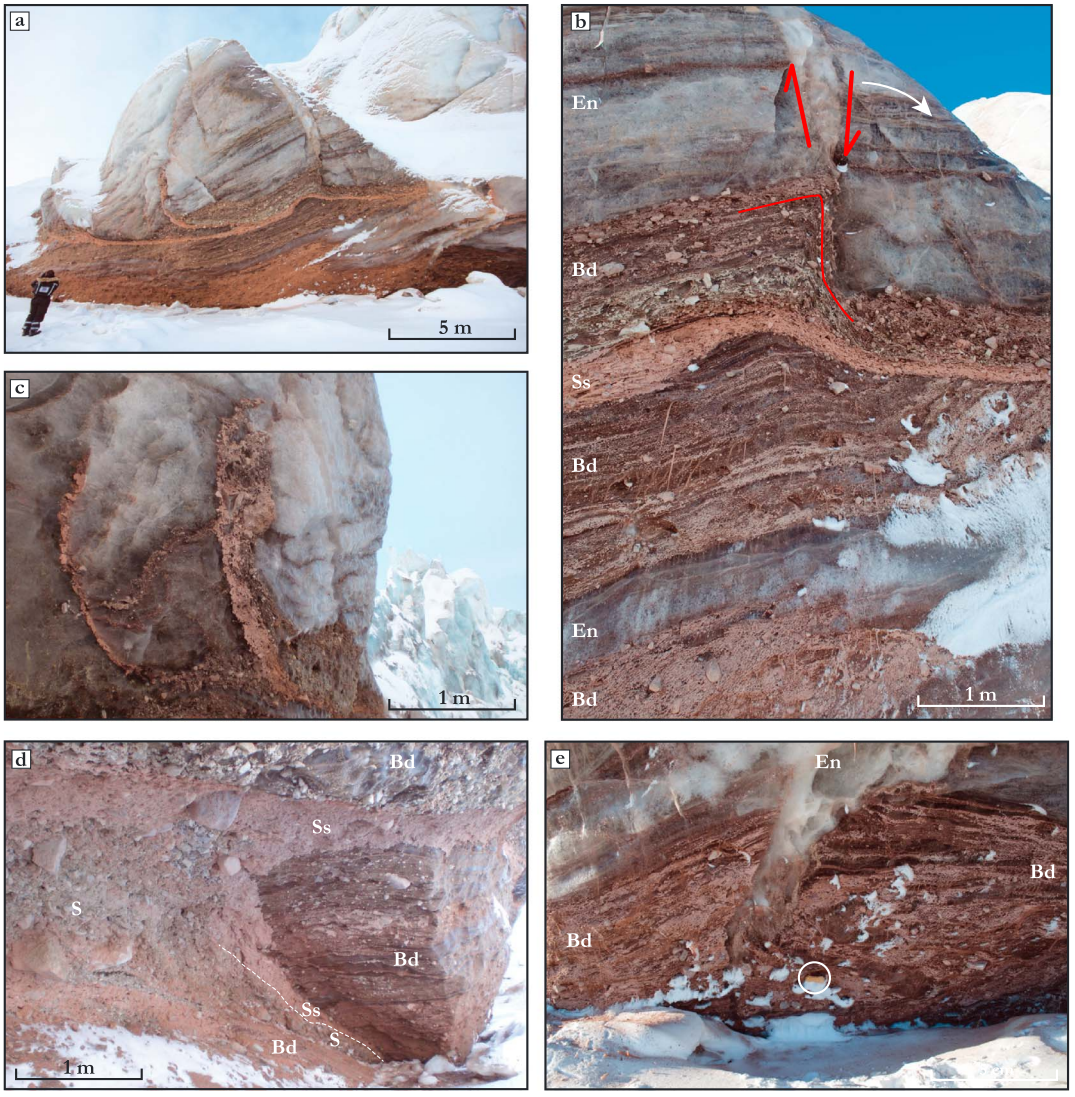

Figure 6. Basal ice stratigraphy at NW section. Ss = solid stratified; S = solid; Bd = banded; En = englacial. (a) Overview of right-hand end of section (photo: Kathrin Naegeli). (b) Inclined, asymmetric z-shaped fold within banded subfacies (outlined in red) overlying open fold in solid stratified layer. Note also the normal fault in the overlying englacial facies and slight lateral rotational movement of hanging wall away from foot wall (white arrow). (c) Examples of vertical intrusions of solid stratified and banded subfacies into overlying englacial facies. (d) Truncation of banded subfacies ice by solid stratified and solid subfacies ice. White dashed line divides the two latter subfacies. (e) Banded subfacies ice truncated by englacial facies ice. Twenty centimeter brush circled for scale.

throughout and in some places there is evidence that the contact between the two is unconformable, such as between 70 and 80 m (as) where the banded subfacies laminae are truncated by the solid stratified subfacies (Figures 2a and 6b). The solid stratified subfacies is typically overlain by a further layer of banded subfacies ice. Throughout the section, the lower banded subfacies layers (underlying the solid stratified subfacies) are bisected by discontinuous layers of englacial facies ice (Figures 2a, 6a, and 6b). The lower banded subfacies layer is truncated by englacial facies ice in at least two places at the right-hand (NE) end of the section, at ~70 m (as) (Figure 6b) and 75 m (as) (Figure 6e). Both the solid stratified and the banded subfacies also form subvertical and occasionally overturned intrusions into the overlying englacial facies, typically 1–2 m long (Figure 2a).

Between ~30 and 45 m (as), the lower banded subfacies layer is truncated by a ~1 m thick combined layer of solid stratified and solid subfacies ice extending from the base of the section (Figures 2a and 6d). These

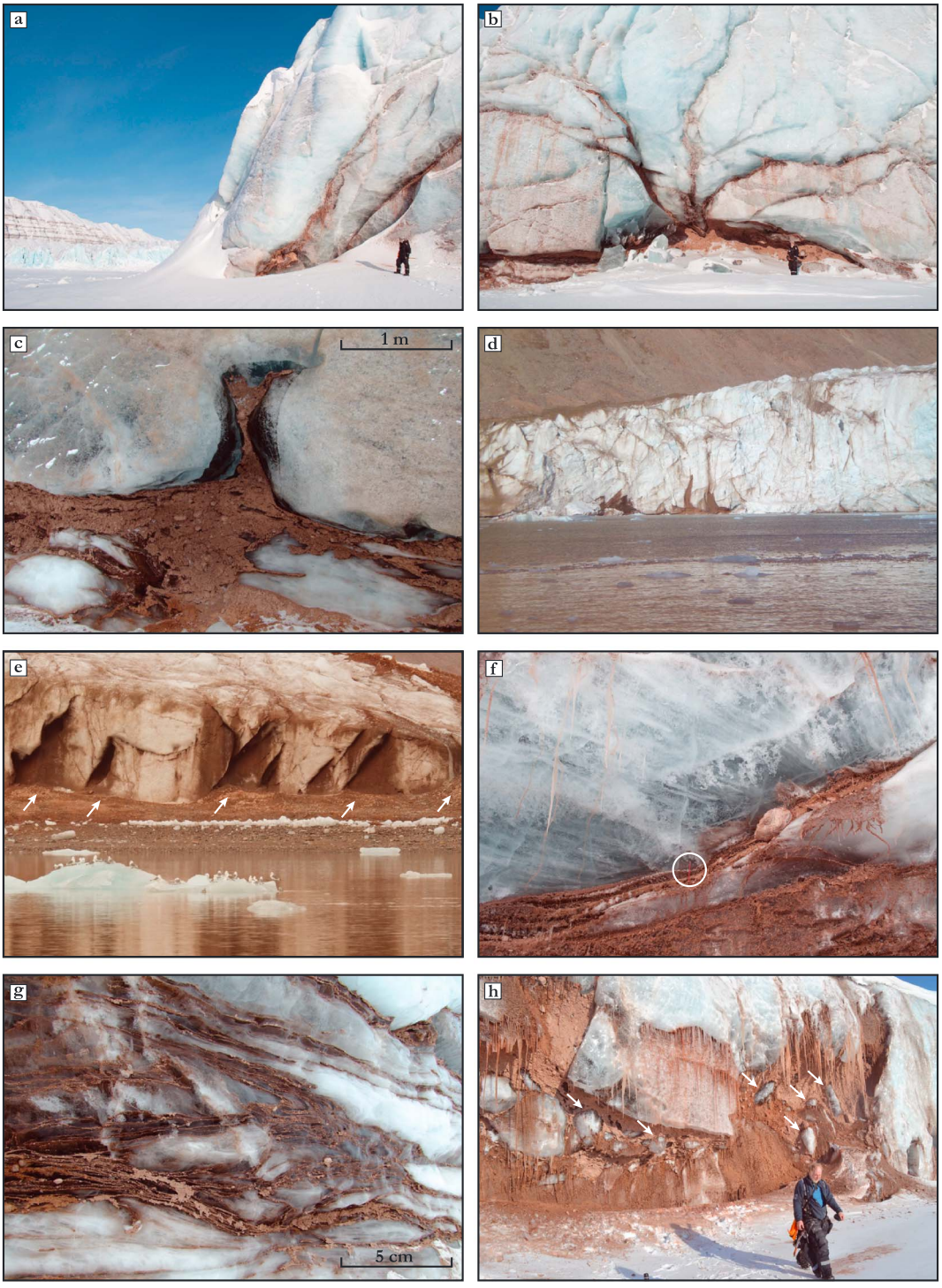

Figure 7. Debris-rich englacial structures. (a) Thin debris-rich structures, SE-A section. (b) Thin debris-rich structure extending from area of solid stratified facies ice, SE-A section. (c) Vertical diapiric-like debris-rich structure at SE-A with dispersed facies ice border. (d) Vertical debris-rich structures in ice cliff close to NW section. Ice cliff is ~30 m high. (e) Small ridges (arrowed) emanating from inclined debris-rich structures, SE-B section (photo: Andy Hodson). (f) Debris-rich structure truncating bubble stratification in dispersed facies ice, SE-A section. Pencil circled for scale. (g) Recumbent fold within banded subfacies, SE-A section. (h) Apron entrainment of englacial ice blocks (arrowed) into stratified ice near the SE-A section. Photos in Figures 7c and 7g: Roberto Colucci.

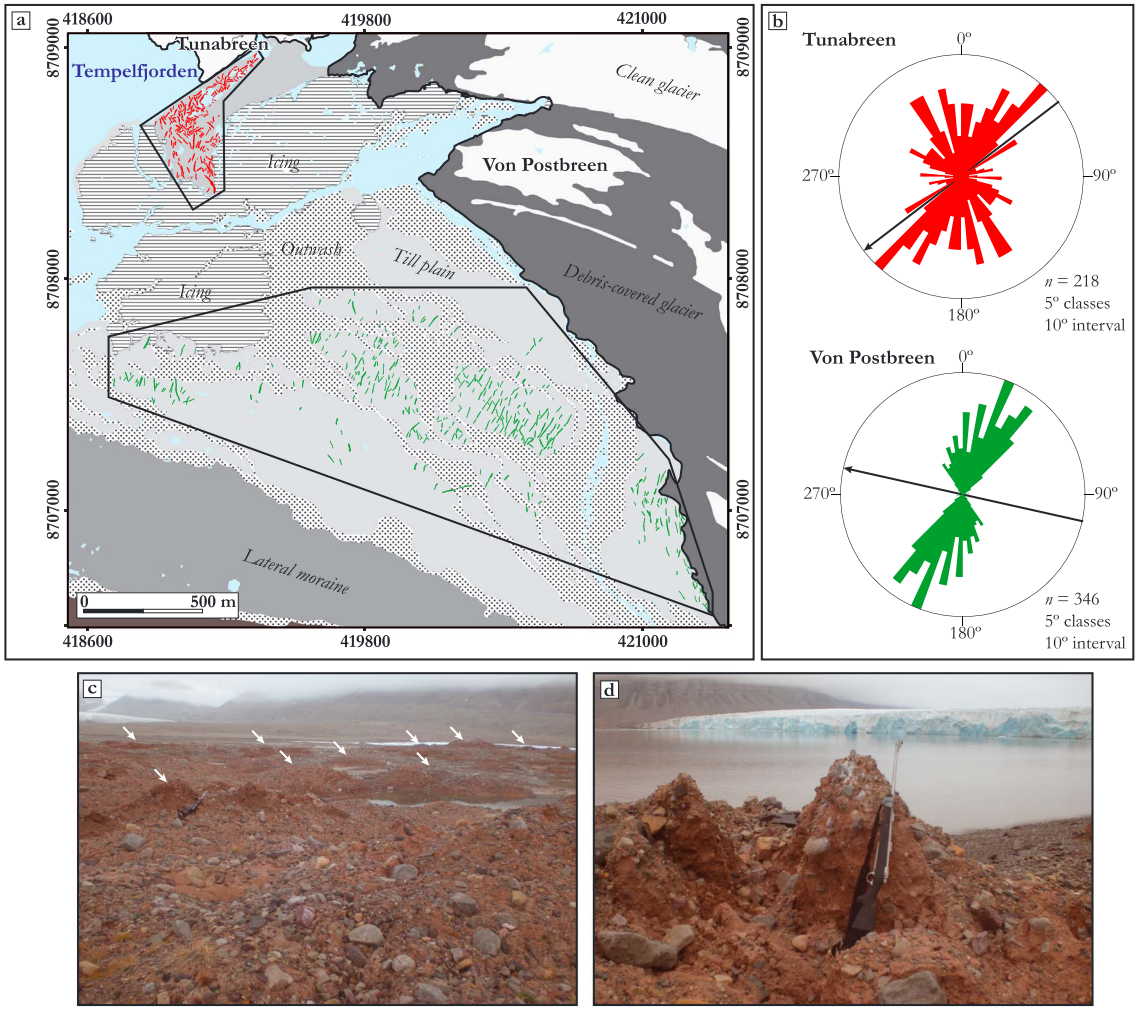

Figure 8. Terrestrial geometrical ridge networks. (a) Map of ridges associated with Tunabreen (in red) and Von Postbreen (in green). (b) Rose diagrams of ridge orientations. Black arrows on rose diagrams show centerline ice flow directions at the terminus. (c) View across Tunabreen ridges (arrowed) toward Von Postbreen (top left). The diamict clast shape samples in Figure 4 are from this group of ridges. (d) Sharp-crested ridge close to Tempelfjorden shore with Tunabreen in the background.

subfacies thicken upward and coalesce with the continuous solid stratified subfacies layer, forming a 2 m thick unit between upper and lower banded subfacies layers.

4.2.2. SE Sections

The SE sections are less debris-rich than the NW section, typified by stratified facies layers and debris-rich structures surrounded by englacial facies ice (Figures 2b and 2c). The debris-rich structures display a variety of morphologies and alignments along the SE sections. A large number of these are <30 cm thick and attenuate toward the top of the structure, which is typically at 10–15 m up section (Figures 2b, 2c, and 7a–7c). In many cases the debris-rich structures extend upward into englacial ice from more-extensive areas of stratified facies ice at their base (Figures 7b and 7c). Thin debris laminae of fines and clots also commonly emanate from the main structure, often into bordering dispersed facies ice (e.g., arrowed in Figure 3b), and many of these are aligned subparallel to the surface of the structures. The structures often contain small clean ice lenses, and in several places, areas of sorted sands and gravels were observed. The debris-rich structures exhibit a variety of orientations, dips, and dip directions (Figure 2c). In general, the debris-rich structures at the SE sections are inclined (Figures 2, 7a, 7b, and 7e), but there are also examples of near-vertical structures both here (Figure 7c) and within the ice cliff near the NW section (Figure 7d). The debris-rich structures are typically bordered by dispersed facies ice, which is often bubble-free immediately adjacent to the structure but grades into increasingly bubble-rich ice over a distance of tens of centimeters (e.g., Figures 3b, 3c, and 7f).

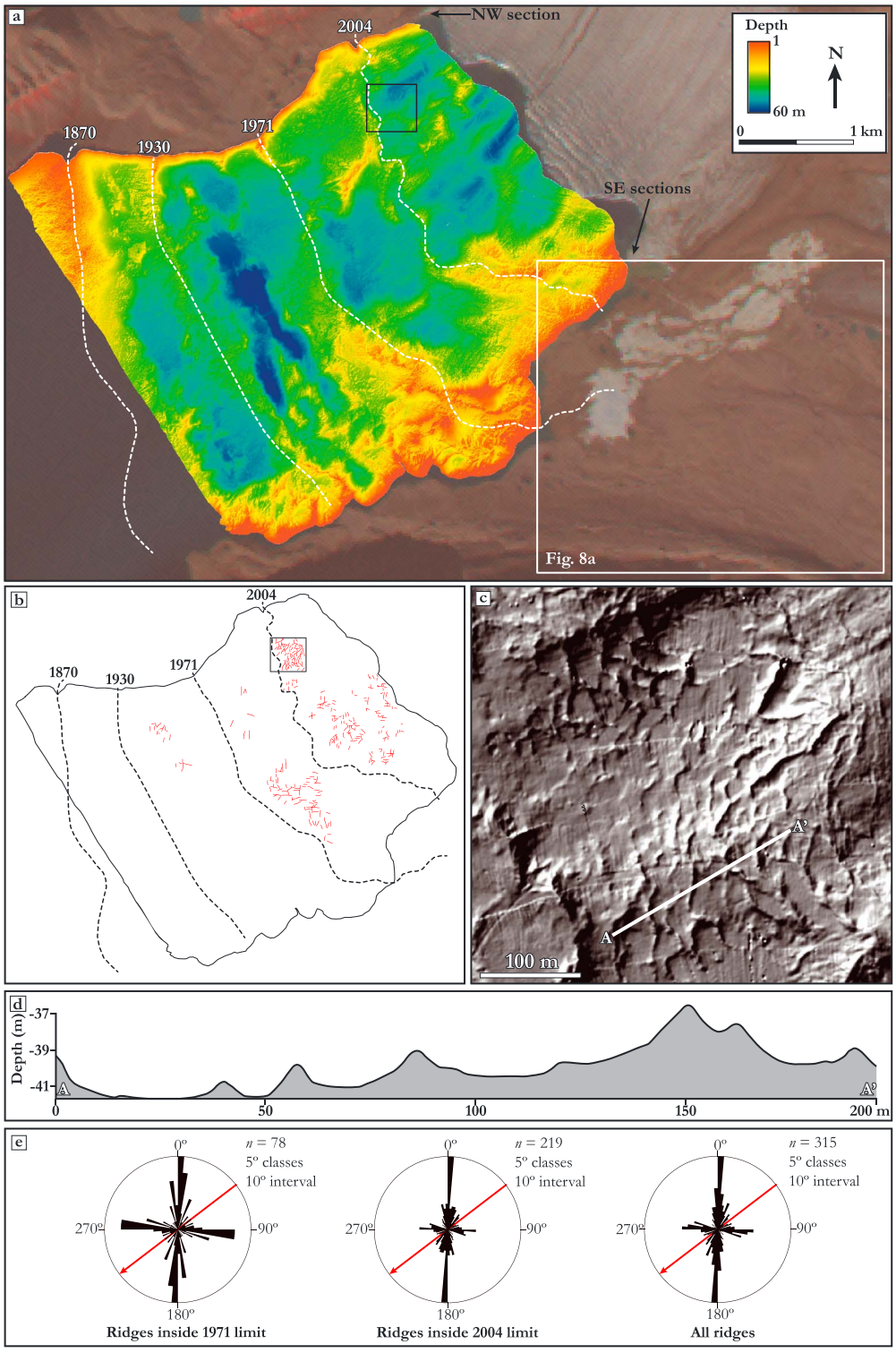

Figure 9. Submarine geometrical ridge networks in Tempelfjorden. (a) Swath bathymetry of inner Tempelfjorden with 2010 ASTER (Advanced Spaceborne Thermal Emission and Reflection Radiometer) image as background. 1870, 1930, 1971, and 2004 surge limits are shown. Black rectangle delimits area shown in detail in (c); white rectangle shows area mapped in Figure 8a. (b) Mapped submarine geometrical ridges. Black rectangle delimits area shown in detail in Figure 9c. (c) Shaded relief image of area delimited by the black rectangles in Figures 9a and 9b. Note the thin ridges displaying a variety of alignments. Transection A-A′ shown in Figure 9d. (d) Profile along transection A-A′ from Figure 9c. (e) Rose diagrams of submarine geometrical ridge orientations. Red arrows show centerline ice flow direction at the margin of Tunabreen.

A complex stratigraphy of intercalated layers of stratified, (~1–50 cm thick) dispersed, and englacial facies ice exhibiting clear evidence for deformation in the form of folds and the stacking of units is also evident at the SE sections (Figures 3f and 7f–7h). The clearest exposure of this is at the SE-A section between ~35 and 90 m (as) (Figure 2b). The order and structure of the intercalations is variable, ranging from thin (<5 cm) bands of solid stratified and banded subfacies ice within the meters thick englacial facies (Figures 7f and 7g) to tens of centimeters thick solid stratified ice interspersed with englacial facies layers of <10 cm. The translucent nature of the clean ice layers within the banded facies is advantageous as it often allows folds to be observed in three dimensions, and various types are evident, ranging from steeply inclined to recumbent (Figure 3f), with tight to isoclinal interlimb angles and typically asymmetrical limbs. Boudinage is also common within the banded subfacies, forming augen-like rings of debris within the host englacial facies (e.g., Figure 10a in *Fleming et al.* [2013]). The vergence direction of the folds is variable and in some cases appears to be in two opposite directions when viewed in the two-dimensional ice face, implying that the fold hinges are curvilinear (Figure 7g).

When parts of the SE sections were visited in summer, small (<1 m high) ridges were melting-out from the base of debris-rich structures (Figure 7e). These ridges consisted of poorly sorted matrix-supported diamict, visually indistinguishable from the debris within the stratified facies ice and terrestrial geometrical ridges (see section 4.3).

4.3. Geometrical Ridge Networks

Linear ridges oriented in several different directions and often intersecting each other form geometrical networks at the margins of Tunabreen and Von Postbreen, both in a terrestrial position (Figure 8) and on the fjord floor (Figure 9).

4.3.1. Terrestrial Ridge Networks

Ridges on the SE side of Tempelfjorden are concentrated into two distinct populations: a dense grouping located immediately adjacent to the fjord and close to the position reached in 2004 by Tunabreen (red in Figure 8a), and a larger group distributed across the Von Postbreen foreland (green in Figure 8a). The Tunabreen ridges are typically sharp crested and up to 3 m high, display a range of orientations (Figure 8b), and are composed of a reddish-brown matrix-supported diamict (Figures 8c and 8d) with predominantly subangular, striated clasts (Figure 5a). The Von Postbreen ridges are typically 1-3 m high and also consist of matrix-supported diamict, although of a lighter brown shade than the Tunabreen ridges. The orientations are much less variable than at Tunabreen, with ridges oriented dominantly perpendicular and subperpendicular to the general ice flow direction (Figure 8b).

4.3.2. Submarine Ridge Networks

On the fjord floor, the ridges range from 0.5 to 4 high and have a similar planform morphology to those in a terrestrial position (Figure 9c). The ridges are predominantly oriented at a 45° offset from the centerline ice flow direction of Tunabreen (Figure 9e) and can be subdivided into three populations based on their location relative to surge limits: the largest group (219 ridges) is located inside the 2004 surge limit, 78 ridges are located outside the 2004 limit but within the 1971 limit, and 17 ridges are located outside the 1971 limit but inside the 1930 limit (Figure 9b). No ridges could be identified between the 1930 and 1870 limits or beyond.

5. Interpretation and Discussion

5.1. Formation of Ice Facies

5.1.1. Englacial Facies

This facies comprises the bulk of the glacier and the upper parts of the NW and SE sections and is interpreted as stratified meteoric ice formed by the firnification of snow in the accumulation area. The mean $\delta^{18}O$ composition of the englacial facies (−15.34‰; Table 2) is similar to 11 year running mean values for meteoric ice from the Lomonosovfonna ice core record (typically between −15 and −16‰) [*Divine et al.*, 2008].

5.1.2. Dispersed Facies

Dispersed ice and the descriptively similar facies termed "clotted" [*Knight*, 1987; *Sugden et al.*, 1987] and "clear" [*Sharp et al.*, 1994; *Hubbard and Sharp*, 1995; *Hubbard et al.*, 2000] in previous studies are typically interpreted to have formed through either sedimentary [e.g., *Lawson*, 1979; *Knight*, 1987; *Sugden et al.*, 1987] or tectonic [e.g., *Sharp et al.*, 1994; *Hubbard et al.*, 2000; *Waller et al.*, 2000; *Cook et al.*, 2011] processes. At Tunabreen, a combination of both processes is proposed, characterized by strain-induced metamorphism of meteoric ice

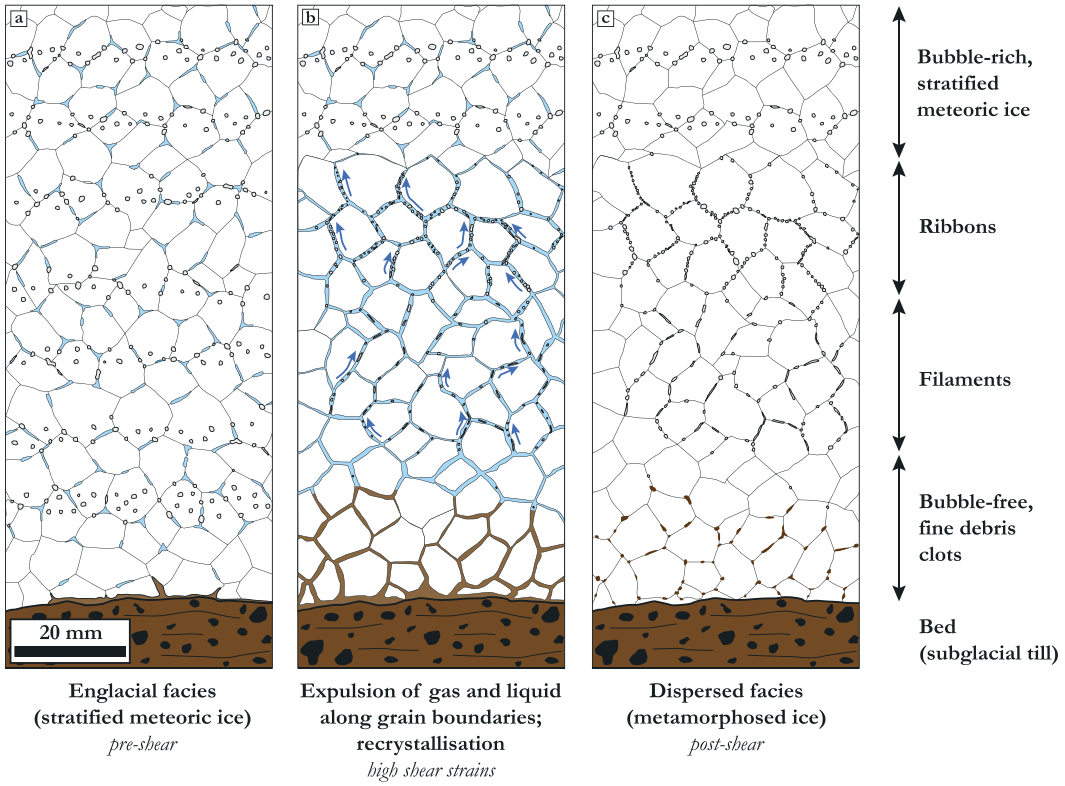

Figure 10. Schematic diagram showing inferred formation of dispersed facies ice due to strain-induced metamorphism of englacial facies ice. (a) Englacial facies (meteoric) ice in close proximity to the bed presurge. (b) Strain-induced metamorphism of the englacial facies ice during the surge results in recrystallization and the expulsion of gas and liquid via the intercrystalline vein network. (c) Dispersed (metamorphosed) facies ice.

in close proximity to the glacier bed and/or debris-rich basal ice. The very clear, bubble-poor nature of much of this facies is consistent with the expulsion of gas during ice deformation [*Hubbard and Sharp*, 1995]. This deformation has been suggested to involve melting and refreezing at grain boundaries [*Kamb and LaChapelle*, 1964] and the removal of gas along triple-grain veins [*Hubbard et al.*, 2000]. The bubble structures which trace the outline of ice crystals are consistent with this process of gas expulsion (Figure 3c and 10). This pattern continues as the bubble structures grade into planar ribbons, although the crystal boundaries are more diffuse. Occasional larger bubbles and dispersed bubble clouds may represent remnants of meteoric ice where gas expulsion was incomplete [*Hubbard and Sharp*, 1995]. Further, the fine-grained sediment within the dispersed facies is consistent with turbid water flowing within a vein network between crystals [*Lliboutry*, 1993]. The proximity of the dispersed facies to debris-rich stratified facies ice in almost all occurrences suggests this debris is sourced directly from the fines that comprise the diamict matrix (Figure 5c). Tectonic deformation is evident within the thin debris laminae in the dispersed facies, which often display a strong linear component indicative of shear (Figure 3b). Such features within basal ice sequences have been termed stretching lineations [e.g., *Fleming et al.*, 2013; *Lovell et al.*, 2015] and are similar to stringers commonly described from glacitectonized sediments [e.g., *Roberts and Hart*, 2005].

The mean $\delta^{18}O$ value for the dispersed facies (−14.36‰) is statistically indistinguishable from that for the englacial facies (−15.34‰) (Table 2). The dispersed facies data do not produce a freezing slope on a coisotopic plot; the absence of a freezing slope indicates that the dispersed facies is not formed by bulk adfreezing of water from a single initial source of limited extent with a specific isotopic composition [*Souchez et al.*, 1988]. This suggests that grain boundary melting and refreezing is not confined to one cycle (e.g., bulk adfreezing) sourced only from the englacial facies but may be the result of multiple melting and partial refreezing events with numerous water sources in an open system [*Sharp et al.*, 1994; *Cook et al.*, 2010]. This process is envisaged as partial melting of ice crystals, followed by redistribution of water via flow along intercrystalline veins and eventually partial refreezing and recrystallization. This may be

reflected by the high ranges in measured δ^{18}O and δD values (3.51‰ and 23.82‰, respectively) [cf. *Souchez et al.*, 1988], which can be explained by fractionation of the initial partial melt during subsequent refreezing. This creates new ice that is initially heavy and subsequently becomes progressively lighter than the isotopic composition of the initial water. A high range in δ^{18}O and δD would therefore be consistent with differential degrees of refreezing occurring at the sample scale within the dispersed facies.

5.1.3. Stratified Facies

5.1.3.1. Solid Stratified Subfacies

The debris characteristics of the solid stratified subfacies are consistent with frozen subglacial till [*Sugden et al.*, 1987; *Sharp et al.*, 1994; *Evans et al.*, 2006]. Regelation is unlikely to have been responsible for its formation as it rarely produces layers >0.1 m thick [*Nye*, 1970; *Hubbard and Sharp*, 1993] and is typically associated with low debris concentrations [*Kamb and LaChapelle*, 1964; *Hubbard*, 1991], which contrasts with the thickness and high debris concentrations of the solid stratified subfacies. Vertical regelation into the bed is most effective at incorporating coarse-grained, clast-supported debris [*Alley et al.*, 1997], which contrasts with the silt-rich matrix of the solid stratified subfacies (Figure 5c). Glacihydraulic supercooling has been invoked as a formation mechanism for debris-rich ice that shares some physical similarities with the solid stratified subfacies, including polymodal grain size distribution, medium to high debris concentrations, interstitial ice, small areas of sorted sediment, and overall facies thicknesses of >0.5 m [*Lawson et al.*, 1998; *Cook et al.*, 2010]. However, these examples were also associated with additional features thought to be diagnostic of supercooling, e.g., upwelling vents, anchor ice terraces, and fractures filled with platy ice [*Evenson et al.*, 1999], none of which are observed at Tunabreen.

Based on this, the favored interpretation is that the solid stratified subfacies is a subglacial till that has frozen on due to conductive cooling where the ice is sufficiently thin, such as at the margin [*Weertman*, 1961; *Alley et al.*, 1997]. This process describes the situation where the 0°C isotherm migrates downward into subglacial material, forcing a switch from net basal melting to net basal freezing [*Alley et al.*, 1997]. In the case of polythermal surge-type glaciers, rapid freeze-on occurs upon surge termination as a cold wave propagates downward through the newly thinned and heavily crevassed glacier [cf. *Alley et al.*, 1997; *Larsen et al.*, 2010].

The stable isotope data show that the stratified facies is enhanced in heavy ^{18}O relative to englacial facies ice (Table 2 and Figure 5). This is consistent with both a supercooling origin [*Lawson et al.*, 1998; *Swift et al.*, 2006; *Cook et al.*, 2010] and with ice formation through refreezing of water in close association with a debris-rich bed [*Lawson*, 1979; *Knight*, 1989; *Hubbard and Sharp*, 1993]. It has been demonstrated that differentiating between these is possible when the data are plotted coisotopically, [e.g., *Jouzel and Souchez*, 1982; *Souchez and Jouzel*, 1984; *Cook et al.*, 2010]; however, there is no statistically significant slope defined by the Tunabreen coisotopic data. This indicates that the isotopic composition is complex and may reflect a combination of processes and a range of different parent waters with variable isotopic compositions [*Hubbard and Sharp*, 1993; *Sharp et al.*, 1994; *Knight*, 1997; *Swift et al.*, 2006].

5.1.3.2. Banded Subfacies

The characteristics of the banded subfacies are also consistent with refreezing at the glacier base, producing thin, discontinuous layers of alternating debris-rich and clean ice [*Sugden et al.*, 1987; *Sharp et al.*, 1994; *Hubbard and Sharp*, 1995; *Waller et al.*, 2000; *Larsen et al.*, 2010]. This can indicate a freeze-on [*Weertman*, 1961] and/or regelation [*Hubbard and Sharp*, 1993] origin. Regelation is associated with typical debris concentrations of ~5–10% [*Kamb and LaChapelle*, 1964; *Alley et al.*, 1997], which is consistent with the lowest measured concentration for the stratified facies (9.6%). Debris concentrations at the NW section are typically observed to be higher relative to this, probably closer to the 31% measured at the SE-B section. This higher debris concentration, and the textural characteristics of this debris (e.g., polymodal grain size distribution and edge-rounded clasts; Figure 5), indicates that basal freeze-on is also likely to have been important. Therefore, a combination of freeze-on and regelation is favored for the formation of the banded subfacies, similar to the interpretations of *Larsen et al.* [2010]. However, these processes alone are unlikely to form the up to 10 m thick units at the NW section (Figure 2a). We suggest that the folding and stacking of originally thin layers (Figure 3f) and the intercalation of englacial layers and debris-rich ice (Figures 2a and 7g) indicate that significant postformational tectonic thickening has occurred within the banded subfacies.

5.1.3.3. Solid Subfacies

The structureless character of the solid subfacies ice and its composition of almost entirely angular to subangular clasts of a single lithology (limestone) are indicative of *en masse* entrainment by freeze-on

processes [*Lawson*, 1979; *Lawson et al*., 1998] of localized material that has probably undergone very little transport at the glacier bed.

5.2. Formation of Basal Ice Stratigraphy Linked to Surge Processes

5.2.1. Dispersed Facies Formation

There are two possible explanations for the formation of the dispersed facies due to strain-induced metamorphism of meteoric ice and its link to surge cycles: (1) The facies forms by slow ductile deformation throughout the quiescent phase, which allows sufficient time to expel the gas bubbles and redistribute the predominantly fine-grained sediment, and is not notably altered (other than some thickening) during the active phase. (2) The facies forms almost entirely during the limited timeframe of active phase deformation as meteoric ice is subjected to intense and variable strain in close proximity to the bed during the surge. This creates a temperate "mushy" zone [cf. *Fowler*, 1984] and promotes recrystallization and the migration of gas bubbles and turbid water (sourced from the saturated bed) around grain boundaries and away from the shear zone. This is also apparent where meteoric ice blocks have been sheared over each other, creating thin borders of dispersed ice immediately adjacent to the shear plane (e.g., Figure 7c). We favor interpretation (2) because, first, at the sites examined at the grounded lateral margins of the glacier, there appears to have been little or no movement of the ice since surge termination. If the dispersed facies is related to quiescent phase flow, it could be expected that the areas where it is present would be slowly moving and being subjected to ongoing ductile deformation, which is not apparent up to eight years after surge termination. Second, if the dispersed facies is a quiescent phase signature, then it should be overprinted on the other facies within the basal sequence. However, it occurs in distinct structural relationship with the others, i.e., at the margins of stacked blocks and immediately adjacent to shear planes. Based on this, it seems most likely that the metamorphism occurs during the active surge phase in conjunction with the deformation of the entire basal sequence.

5.2.2. Stratified Facies Formation

The debris-rich portion of basal ice sequences in warm-based glaciers tends to be relatively thin (~1 m) [*Kirkbride*, 1995; *Hubbard et al*., 2000], while in ice sheets it can be much thicker (~10–15 m) [*Gow et al*., 1979; *Herron and Langway*, 1979; *Carsey et al*., 2002; *Christoffersen et al*., 2006]. Basal ice sequences reported from the margins of surging glaciers lie generally somewhere in between. *Christoffersen et al*. [2006] modeled the freezing process which would occur at the ice-bed interface (typically beneath ice streams) when the temperature gradient within the ice is sufficiently steep to induce basal freeze-on. The key control on both the freezing rate and the debris concentration of the basal ice layer was the water availability. Where sufficient water is available to satisfy the temperature gradient-dictated freezing rate, little sediment is incorporated into the basal ice and freezing rates are typically low (~1 mm a^{-1}). When around half the water needed is available, freezing rates increase (1–3 mm a^{-1}) and likewise debris concentrations. The highest freezing rates (~6 mm a^{-1}) are experienced when only till pore water is available for freezing and debris concentrations are high (>60% by volume). Only the highest freezing rates are sufficient to explain thick debris-rich basal ice sequences and only then if freezing is sustained for long periods. The quiescent phase length for Tunabreen (~40 years) would only provide time for the freeze on of ~0.25 m of basal ice. It is possible that ice could accrete across multiple quiescent-surge cycles, provided not all the basal ice formed during the quiescent phase was melted during the subsequent surge. However, freeze-on would be most effective and long lived in the stagnant ice found toward the snout during the quiescent phase, which would limit the number of cycles over which this could occur and the likely thicknesses attainable. The kinematics of surging point to other explanations for the observed basal ice stratigraphy.

5.2.2.1. Thickening and Stacking of Basal Ice Facies

There is evidence for the folding and stacking of basal ice resulting in overall thickening and the formation of complex facies architecture [e.g., *Knight*, 1989; *Sharp et al*., 1994; *Waller et al*., 2000; *Larsen et al*., 2010]. For the NW section this is clearest where solid stratified subfacies ice, interpreted as frozen-on subglacial till (and therefore representing stratigraphically the lowermost basal ice unit), has been elevated on top of both the banded subfacies and the englacial facies ice (Figure 2a). The stacking is particularly obvious at the right-hand end of the NW section (Figures 2a, 6a, and 6b). The banded subfacies reaches a maximum thickness of ~10 m toward the left-hand end of the section, where folding and dislocation of individual laminae can be clearly identified (Figure 2a). The solid stratified facies has also been thrust up

over banded facies ice at ~30–45 m (as), forming the clear truncation extending from the base of the section. The basal stratigraphy at the NW section is interpreted to be the result of active surging ice encountering inactive ice and the bed of the glacier in a terrestrial position at the side of the fjord, resulting in units being sheared over each other and stacked. Observations of such processes can be seen within the time-lapse imagery of the 2005 Paulabreen surge [*Kristensen and Benn*, 2012], which shows the movement of ice blocks over each other and the incorporation of debris-rich inactive ice at the terrestrial margin.

Tectonic thickening is also very clear at the SE-A section, particularly between ~35 and 90 m (as) (Figure 2b). Here there are complex intercalations of the stratified, englacial, and dispersed facies (Figure 7g). Evidence for ductile deformation is clearly preserved in the form of folding and boudinage [e.g., *Sharp et al*., 1994; *Ó Cofaigh and Evans*, 2001], typically identified within the thin laminae of the banded subfacies (Figures 3f and 7g). The different styles of folding record ductile deformation within the lower parts of the section, resulting in thickening of individual facies and of the overall basal sequence [e.g., *Sharp et al*., 1994; *Waller et al*., 2000]. The augen-like rings within the areas of boudinage are interpreted as the fold noses of sheath folds exposed in the 2-D section, reflecting highly noncylindrical folding and indicating that increasing shear strain has resulted in the fold hinges being stretched in a direction perpendicular to the exposure face. The broadly N-S oriented axes of the sheath folds are aligned with the localized ice flow direction in this area as ice splayed laterally into a small embayment and onto the terrestrial margin, as recorded by surface foliation (Figure 1), and also matches fabric derived from AMS measurements at the section [*Fleming et al*., 2013]. In addition to the ductile deformation recorded by complex folding within the shear zone, there is also evidence for brittle deformation in the form of stacking and shearing of englacial facies blocks as they are fractured and then thrust up over each other.

5.2.2.2. Apron Entrainment

There is evidence for apron entrainment in several places, both of ice marginal material and of ice and debris reworked from within the glacier. At the SE margin, large (up to 1 m diameter) meteoric ice blocks are observed within the thicker areas of solid stratified subfacies (Figure 7h), which are suggested to have broken off and fallen from the ice cliff, and then been overridden and entrained. Apron entrainment is likely to have been responsible for the formation of the solid subfacies (at the NW section), interpreted as locally derived supraglacial or paraglacial material that has been entrained into the subglacial till, before both have been stacked, by folding and faulting, up over banded subfacies ice at ~30–45 m (as) (Figures 2a and 6d). These processes are consistent with observations from Paulabreen, which shows continuous failure and dry calving of ice across the entire terrestrial margin, as well as the deformation and overriding of debris-rich stagnant ice and ice marginal sediments [*Kristensen and Benn*, 2012].

5.3. Formation of Debris-Rich Englacial Structures

Debris-rich structures exposed at the margin of Tunabreen vary in size, thickness, morphology, orientation, and dip, but are all predominantly composed of solid stratified subfacies ice (frozen subglacial till). We suggest that several mechanisms are responsible for their formation based on observed characteristics. It is also apparent that more than one mechanism, acting at different times, can influence individual structure formation.

5.3.1. Crevasse Squeezes

Vertical and near-vertical structures, which rarely extend more than ~5 m above the ice cliff base at Tunabreen (Figures 7c and 7d), are best explained by the process of saturated and deformable till being squeezed, under pressure, into basal crevasses, known as crevasse squeezes (Figure 11a) [e.g., *Rea and Evans*, 2011]. The tectonic stresses experienced during surges as ice undergoes both extensional and compressional flow leads to the development of widespread crevassing, which is clearly displayed on the glacier surface (Figure 1). The glacier base also fractures and in some cases crevasses can be full depth [*Rea and Evans*, 2011]. The combination of crevasses open at the bed and the availability of saturated, soft, and deformable sediment, particularly in a glacimarine setting, present a clear opportunity for the formation of crevasse squeezes as the glacier lowers back down into its bed upon surge termination [*Sharp*, 1985]. It is notable that vertical and near-vertical structures are largely absent from the NW and SE sections, both of which are at the terrestrial margins of the glacier, but are observed above the waterline within the tidewater ice cliff (Figure 7d). We suggest that this reflects the dominant tectonic stress regimes active across the glacier during the surge: at the terrestrial margins, surging ice encountered topographic obstructions, e.g., inactive ice and moraines, so stresses remained compressive, favoring the development of thrusts,

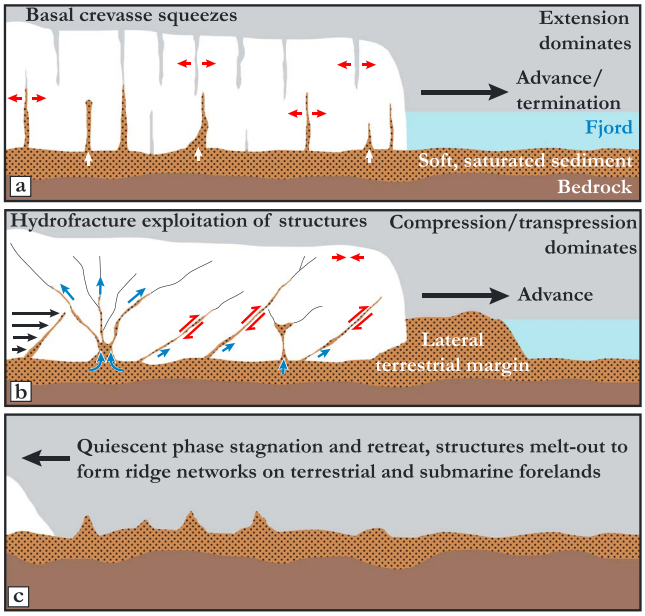

Figure 11. Debris-rich englacial structure formation. (a) Crevasse squeezes formed in an extensional stress regime. (b) Hydrofracture exploitation (blue arrows) of thrust faults, thrust-style displacement (TSD) of reoriented crevasse squeezes and other preexisting fractures in a compressive/ transpressive stress regime. (c) Melted-out geometrical ridge network.

thrust-style displacement (TSD), hydrofractures, and longitudinal crevasses. By contrast, ice reaching the calving front, where basal traction is negligible, would have experienced extensional flow, facilitating the opening of Mode 1 crevasses perpendicular to flow [*Rea and Evans*, 2011].

5.3.2. Hydrofracture Exploitation of Shear Planes and Preexisting Fractures

Numerous thin, dipping structures within the SE sections (Figures 2b, 2c, 7a, and 7e) cannot be explained by the crevasse squeeze mechanism, or at least not without the action of other processes. Many of these structures are highly attenuated, extend for tens of meters and display variable dip angles (Figure 2c), and clearly contrast with the vertical and near-vertical crevasse squeezes. These are interpreted as fractures within the ice that have been forced open due to high basal water pressures (>80% of ice overburden pressure) and injected with saturated debris (Figure 11b). In some cases, these fractures are likely to be thrust faults formed within the surging ice in a highly compressional flow regime, as has been reported from several surge-type glaciers [e.g., *Sharp* et al., 1988; *Hambrey and Dowdeswell*, 1997; *Murray et al.*, 1997; *Glasser et al.*, 1998; *Lønne*, 2006; *Larsen et al.*, 2010]. The conditions at the surge front during the active phase can produce very large stress gradients between weakly coupled surging ice with low basal drag (i.e., where the driving stress is not supported by the bed) and surrounding ice with high basal drag. Thrust faults would form as stress is transferred across the low to high basal drag zones. As the hanging wall is sheared over the foot wall, it is possible that some subglacial till could be dragged along the fault, although it is unlikely that this displacement alone would transport debris more than a short distance [*Rea and Evans*, 2011]. However, if basal water pressures and pore water pressures in subglacial till reach ice overburden pressure and the fracture is oriented close to an optimal fracture angle [cf. *Moore et al.*, 2010], then it could be forced open, effectively becoming a hydrofracture and providing a route along which water and saturated debris can escape.

In addition to facilitating the development of debris-rich thrust faults, it is also probable that hydrofractures exploit preexisting weaknesses in the ice. These include crevasse squeeze structures that formed during a previous surge and have then been slowly reoriented in a down-ice direction during the quiescent phase [*Evans and Rea*, 1999; *Woodward et al.*, 2002]. Such inclined till-filled structures present a favorably oriented slip plane that can be exploited during a subsequent surge by TSD [*Rea and Evans*, 2011], particularly under conditions of very high basal water pressures that force the fracture open and allow the injection of water and saturated debris. In the case of both thrust faulting and TSD of reoriented structures, as the hanging wall extends beyond the foot wall it is likely that it will begin to fail and break up as the underlying support is removed. At the margin, this ice may dry-calve into the glacier's path and subsequently be reincorporated at the bed through apron entrainment [*Evans*, 1989].

Hydrofracturing within a compressive stress regime could also exploit other fractures within the ice that are not directly related to thrust faulting or TSD of reoriented extensional crevasses. An example of this is the thin, multibranched structure extending from a large area of subglacial till at its base at ~90 m (as) (Figures 2a and 7b). Basal water pressures in excess of overburden within the saturated till could lead to hydrofracturing of the overlying ice, creating fractures filled with turbid water draining upward from the bed [*Ensminger et al.*, 2001; *Roberts et al.*, 2009; *Rea and Evans*, 2011] (Figure 11b).

Finally, within many of the thrust fault and reoriented crevasse squeeze structures at Tunabreen the debris is oriented in lineations parallel to the plane of the structure, indicating oblique or transverse movement across the fault as well as in a vertical direction. This represents strike-slip movement and suggests that a transpressional glacitectonic regime was active at the terrestrial margins of the surge [*Fleming et al*., 2013]. A transpressional regime is consistent with surging ice splaying laterally into the side of the fjord, as indicated by the foliation orientation (Figure 1), which would accommodate both a vertical and a horizontal component to the slip plane movement. The predominance of shear planes at the lateral terrestrial margins is also consistent with the suggestion that a compressive/transpressive stress regime was dominant in these areas, rather than the extensional regime that is likely to have prevailed toward the center of flow.

5.4. Geometrical Ridge Formation

The formation of landforms that are inherited from structure within the ice has been described from a broad range of settings and is attributed to a number of different processes [cf. *Evans*, 2009]. At the margins of surge-type glaciers, the link between geometrical ridge networks and debris-rich englacial structures has been made by a number of studies [e.g., *Gripp*, 1929; *Sharp*, 1985; *Boulton et al*., 1996; *Bennett et al*., 1996; *Glasser et al*., 1998; *Evans and Rea*, 1999; *Rea and Evans*, 2011]. Low ridges of diamict, sedimentologically identical to that within the englacial structures and interpreted as subglacial till, were observed melting-out at Tunabreen from dipping structures at the SE sections (Figure 7e). The diamict within these ridges is also identical to that within the population of terrestrial ridges at the Tunabreen margin (Figures 3b, 4a, and 8d), and the spacing between ridges is of a similar order (~2–5 m). Based on this, we suggest that the Tunabreen ridges are also likely to be melted-out englacial till-filled structures, but associated with the previous (1970s) surge, as the area was not reached by ice in 2004 (Figure 1). The population of diamict-filled ridges on the Von Postbreen foreland (Figure 8a) are similarly inferred to relate to subglacial debris-rich structures entrained during the 1870s surge of Von Postbreen. It is also logical, therefore, that the submarine geometrical ridges in Tempelfjorden (Figure 9), which are of a similar scale and morphology to both sets of terrestrial ridges and have a similar spatial arrangement to the Von Postbreen ridges, formed in the same way [e.g., *Solheim and Pfirman*, 1985; *Ottesen and Dowdeswell*, 2006; *Ottesen et al*., 2008; *Flink et al*., 2015].

It is possible to go a step further and attempt to link different ridge populations to different formational mechanisms of the englacial structures from which they are inherited, and thereby to link ridges to specific tectonically controlled debris entrainment processes that are active during surges. This is largely based on the location and spatial arrangement of the ridge networks and is important because geometrical ridge networks are typically interpreted as having a crevasse squeeze origin [e.g., *Sharp*, 1985; *Evans and Rea*, 1999; *Ottesen et al*., 2008], although it is clear that this is not the only process by which till can be entrained and elevated. The Von Postbreen ridges are predominantly oriented at $>60°$ perpendicular to flow, creating a rhombohedral or rectilinear network (Figure 8a). The submarine ridges display two dominant orientations, both perpendicular and longitudinal to flow (Figure 9). These patterns are both consistent with surface crevassing caused by longitudinal stretching and, therefore, it is logical to suggest that the ridges are melted-out crevasse squeezes that originally formed toward the center of a surging glacier, where a simple stress/strain regime dominated by extension existed. The longitudinally aligned ridges in a submarine position probably relate to longitudinal crevasses that opened due to additional splaying at the front of Tunabreen. By contrast, the Tunabreen terrestrial ridges display more variable orientations, with no clear rhombohedral pattern and no dominant alignment perpendicular to centerline ice flow direction (Figures 8a and 8b). We suggest this reflects their location at the terrestrial margin, where it has been established that flow was dominantly compressive/transpressive, and where hydrofracturing, thrust faulting, and TSD were prevalent. Lateral splaying at the SE section would further complicate the stress, fracture, and debris-rich structure orientations in relation to ice flow direction. As a result, the terrestrial Tunabreen ridges display a less distinct spatial pattern than those formed in areas dominated by longitudinal extension.

6. Conclusions

Investigations of debris entrainment and surge geomorphology at the margins of Tunabreen, Svalbard, allow us to make the following observations:

1. Thick (up to 10 m) sequences of debris-rich stratified basal ice are exposed at the lateral terrestrial margins. This ice can be subdivided into a solid stratified subfacies, interpreted as saturated subglacial till that has frozen on, *en masse*, and a banded subfacies characterized by alternations of debris-rich laminae and clean ice layers, interpreted as having initially formed through incremental freeze-on and regelation processes at the ice-bed interface. There is clear evidence for tectonic deformation of the basal sequence at the lateral margins, resulting in an overall thickening of the banded subfacies due to folding and faulting, and the thrusting and stacking of all facies.
2. Debris-poor dispersed facies ice is interpreted as meteoric ice that has undergone strain-induced metamorphism at or close to the bed, most likely during the surge active phase. This facies is characterized by areas of very clear, bubble-free ice that contains isolated debris clots/laminae and some discrete filaments or ribbons of bubbles, which are interpreted as evidence for the expulsion of gas and migration of turbid water away from the bed via the intercrystalline vein network.
3. Debris-rich englacial structures predominantly composed of subglacial till display a variety of morphologies, orientations, and dips. These form during surge active phases and are interpreted as crevasse squeezes and hydrofractures that have exploited shear planes (thrust faults and thrust-style displacement of reoriented crevasse squeezes) and other preexisting weaknesses within the ice.
4. Proglacial geometrical ridge networks develop in both terrestrial and submarine positions as debris-rich englacial structures formed through various processes melt-out during quiescent phase ice stagnation and margin recession.
5. The nature of the basal ice sequence, debris-rich englacial structures, and geometrical ridge networks can provide an insight into spatial patterns of dominant glacitectonic stress regimes during surges. This indicates that a compressional/transpressional regime dominates at the terrestrial lateral margins, particularly where surging ice has splayed laterally and encountered topographic obstacles. Longitudinal extension dominates along the tidewater front and toward the center of surging ice, where velocities are highest.

Acknowledgments

This work was undertaken while H.L. was funded by a NERC PhD studentship (NE/I528050/1) at Queen Mary University of London. Additional funding was acquired from the Queen Mary Postgraduate Research Fund and an Arctic Field Grant from the Research Council of Norway. E.J.F. was funded by a NERC PhD studentship at the University of Birmingham as part of the GAINS (Glacial Activity in Neoproterozoic Svalbard) grant (NE/H004963/1). The bathymetry data for Tempelfjorden is presented with the permission of the Norwegian Hydrographic Service (permission nr. 13/G706; kartverket.no). The following are thanked for fieldwork support: UNIS logistics (particularly Martin Indreiten, Jukka Pekka Ikonen, and Monika Votvik), Andy Hodson, Kathrin Naegeli, Philipp Schuppli, Riccardo Scotti, Roberto Colucci, and Heidi Sevestre, plus all other members of the 2011 UNIS AG-325 Glaciology course. We would also like to thank Ian Boomer for the isotope analyses. Two anonymous reviewers and the Associate Editor, Mike Bentley, are thanked for their constructive comments.

References

Alley, R., K. M. Cuffey, E. B. Evenson, J. C. Strasser, D. E. Lawson, and G. J. Larson (1997), How glaciers entrain and transport basal sediment: Physical constraints, *Quat. Sci. Rev.*, *16*, 1017–1038, doi:10.1016/S0277-3791(97)00034-6.

Andreassen, K., M. Winsborrow, L. R. Bjarnadóttir, and D. C. Rüther (2014), Ice stream retreat dynamics inferred from an assemblage of landforms in the northern Barents Sea, *Quat. Sci. Rev.*, *92*, 246–257, doi:10.1016/j.quascirev.2013.09.015.

Bennett, M. R., M. J. Hambrey, D. Huddart, and J. F. Ghienne (1996), The formation of a geometrical ridge network by the surge-type glacier Kongsvegen, Svalbard, *J. Quat. Sci.*, *11*(6), 437–449, doi:10.1002/(SICI)1099-1417(199611/12)11:6<437::AID-JQS269>3.0.CO;2-J.

Bennett, M. R., D. Huddart, R. I. Waller, N. G. Midgley, S. Gonzalez, and A. Tomio (2004), Styles of ice-marginal deformation at Hagafellsjökull-Eystri, Iceland during the 1998/99 winter-spring surge, *Boreas*, *33*(2), 97–107, doi:10.1111/j.1502-3885.2004.tb01132.x.

Boulton, G., J. J. M. van der Meer, J. K. Hart, D. J. Beets, G. H. J. Ruegg, F. M. van der Wateren, and J. Jarvis (1996), Till and moraine emplacement in a deforming bed surge—An example from a marine environment, *Quat. Sci. Rev.*, *15*, 961–987, doi:10.1016/0277-3791(95)00091-7.

Boulton, G., J. J. M. van der Meer, D. J. Beets, J. K. Hart, and G. H. J. Ruegg (1999), The sedimentary and structural evolution of a recent push moraine complex: Holmstrømbreen, Spitsbergen, *Quat. Sci. Rev.*, *18*, 339–371, doi:10.1016/S0277-3791(98)00068-7.

Brynjólfsson, S., Ó. Ingólfsson, and A. Schomacker (2012), Surge fingerprinting of cirque glaciers at the Tröllaskagi peninsula, North Iceland, *Jökull*, *62*, 151–166.

Carsey, F., A. Behar, A. L. Lane, V. Realmuto, and H. Engelhardt (2002), A borehole camera system for imaging the deep interior of ice sheets, *J. Glaciol.*, *48*(163), 622–628, doi:10.3189/172756502781831124.

Christoffersen, P., J. A. Piotrowski, and N. K. Larsen (2005), Basal processes beneath an Arctic glacier and their geomorphic imprint after a surge, Elisebreen, Svalbard, *Quat. Res.*, *64*, 125–137, doi:10.1016/j.yqres.2005.05.009.

Christoffersen, P., S. Tulaczyk, F. D. Carsey, and A. E. Behar (2006), A quantitative framework for interpretation of basal ice facies formed by ice accretion over subglacial sediment, *J. Geophys. Res.*, *111*, F01017, doi:10.1029/2005JF000363.

Cook, S. J., Z. P. Robinson, I. J. Fairchild, P. G. Knight, R. I. Waller, and I. A. N. Boomer (2010), Role of glaciohydraulic supercooling in the formation of stratified facies basal ice: Svínafellsjökull and Skaftafellsjökull, southeast Iceland, *Boreas*, *39*(1), 24–38, doi:10.1111/j.1502-3885.2009.00112.x.

Cook, S., D. A. Swift, D. J. Graham, and N. G. Midgley (2011), Origin and significance of 'dispersed facies' basal ice: Svínfellsjökull, Iceland, *J. Glaciol.*, *57*(204), 710–720, doi:10.3189/002214311797409703.

Croot, D. G. (1988), Glaciotectonics and surging glaciers: A correlation based on Vestspitsbergen, Svalbard, Norway, in *Glaciotectonics: Forms and Processes*, edited by D. G. Croot, pp. 49–62 , Balkema, Amsterdam.

Divine, D. V., E. Isaksson, V. Pohjola, H. Meijer, R. S. W. van de Wal, T. Martma, J. Moore, B. Sjögren, and F. Godtliebsen (2008), Deuterium excess record from a small Arctic ice cap, *J. Geophys. Res.*, *113*, D19104, doi:10.1029/2008JD010076.

Ensminger, S., R. B. Alley, E. B. Evenson, D. E. Lawson, and G. J. Larson (2001), Basal-crevasse-fill origin of laminated debris bands at Matanuska Glacier, Alaska, U.S.A, *J. Glaciol.*, *47*(158), 412–422, doi:10.3189/172756501781832007.

Evans, D. J. A. (1989), Apron entrainment at the margins of sub-polar glaciers, north-west Ellesmere Island, Canadian High Arctic, *J. Glaciol.*, *35*(121), 317–324.

Evans, D. J. A. (2009), Controlled moraines: Origins, characteristics and palaeoglaciological implications, *Quat. Sci. Rev.*, *28*(3), 183–208, doi:10.1016/j.quascirev.2008.10.024.

Evans, D. J. A., and B. R. Rea (1999), Geomorphology and sedimentology of surging glaciers: A land-systems approach, *Ann. Glaciol.*, *28*, 75–82, doi:10.3189/172756499781821823.

Evans, D. J. A., and B. R. Rea (2005), Surging glacier landsystem, in *Glacial Landsystems*, edited by D. J. A. Evans, pp. 259–288, Hodder Arnold, London.
Evans, D. J. A., D. S. Lemmen, and B. R. Rea (1999), Glacial landsystems of the southwest Laurentide Ice Sheet: Modern Icelandic analogues, *J. Quat. Sci.*, *14*(7), 673–691, doi:10.1002/(SICI)1099-1417(199912)14:7<673::AID-JQS467>3.0.CO;2-#.
Evans, D. J. A., E. R. Phillips, J. F. Hiemstra, and C. A. Auton (2006), Subglacial till: Formation, sedimentary characteristics and classification, *Earth Sci. Rev.*, *78*(1), 115–176, doi:10.1016/j.earscirev.2006.04.001.
Evenson, E. B., D. E. Lawson, J. C. Strasser, G. J. Larson, R. B. Alley, S. L. Ensminger, and W. E. Stevenson (1999), Field evidence for the recognition of glaciohydrologic supercooling, *Geol. Soc. Am. Spec. Pap.*, *337*, 23–35.
Fleming, E. J., H. Lovell, C. T. E. Stevenson, M. S. Petronis, D. I. Benn, M. J. Hambrey, and I. J. Fairchild (2013), Magnetic fabrics of basal ice in a surge-type glacier, *J. Geophys. Res. Earth Surf.*, *118*, 2263–2278, doi:10.1002/jgrf.20144.
Flink, A. E., R. Noormets, N. Kirchner, D. I. Benn, A. Luckman, and H. Lovell (2015), The evolution of a submarine landform record following recent and multiple surges of Tunabreen glacier, Svalbard, *Quat. Sci. Rev.*, *108*, 37–50, doi:10.1016/j.quascirev.2014.11.006.
Fowler, A. C. (1984), On the transport of moisture in polythermal glaciers, *Geophys. Astrophys. Fluid Dyn.*, *28*(2), 99–140, doi:10.1080/03091928408222846.
Glasser, N. F., M. J. Hambrey, K. Crawford, M. R. Bennett, and D. Huddart (1998), The structural glaciology of Kongsvegen, Svalbard, and its role in landform genesis, *J. Glaciol.*, *44*(146), 136–148.
Gow, A. J., S. Epstein, and W. Sheehy (1979), On the origin of stratified debris in ice cores from the bottom of the Antarctic ice sheet, *J. Glaciol.*, *23*, 185–192.
Grant, K. L., C. R. Stokes, and I. S. Evans (2009), Identification and characteristics of surge-type glaciers on Novaya Zemlya, Russian Arctic, *J. Glaciol.*, *55*(194), 960–972, doi:10.3189/002214309790794940.
Gripp, K. (1929), *Glaciologische und Geologische Ergebnisse der Hamburgischen Spitzbergen-Expedition 1927*, Abhandlungen der naturwissenschaftlichen Verein Hamburg, Hamburg.
Hambrey, M., and J. A. Dowdeswell (1997), Structural evolution of a surge-type polythermal glacier: Hessbreen,Svalbard, *Ann. Glaciol.*, *24*, 375–381.
Herron, S., and C. C. Langway Jr. (1979), The debris-laden ice at the bottom of the Greenland Ice Sheet, *J. Glaciol.*, *23*, 193–207.
Hubbard, B. (1991), Freezing-rate effects on the physical characteristics of basal ice formed by net adfreezing, *J. Glaciol.*, *37*(127), 339–347.
Hubbard, B., and M. Sharp (1993), Weertman regelation, multiple refreezing events and the isotopic evolution of the basal ice layer, *J. Glaciol.*, *39*(132), 275–291.
Hubbard, B., and M. Sharp (1995), Basal ice facies and their formation in the Western Alps, *Arct. Alp. Res.*, *27*(4), 301–310.
Hubbard, B., J. L. Tison, L. Janssens, and B. Spiro (2000), Ice-core evidence of the thickness and character of clear-facies basal ice: Glacier de Tsanfleuron, Switzerland, *J. Glaciol.*, *46*(152), 140–150, doi:10.3189/172756500781833250.
Hubbard, B., S. Cook, and H. Coulson (2009), Basal ice facies: A review and unifying approach, *Quat. Sci. Rev.*, *28*, 1956–1969, doi:10.1016/j.quascirev.2009.03.005.
Iverson, N. R. (2000), Sediment entrainment by a soft-bedded glacier: A model based on regelation into the bed, *Earth Surf. Processes Landforms*, *25*, 881–893, doi:10.1002/1096-9837(200008)25:8<881::AID-ESP105>3.0.CO;2-Y.
Jouzel, J., and R. Souchez (1982), Melting-refreezing at the glacier sole and the isotopic composition of the ice, *J. Glaciol.*, *28*(98), 35–42.
Kamb, B., and E. LaChapelle (1964), Direct observation of the mechanism of glacier sliding over bedrock, *J. Glaciol.*, *5*, 159–172.
Kirkbride, M. P. (1995), Ice flow vectors on the debris-mantled Tasman Glacier, 1957-1986, *Geogr. Ann. Ser. A. Phys. Geogr.*, *77*(3), 147–157.
Kjær, K. H., N. J. Korsgaard, and A. Schomacker (2008), Impact of multiple glacier surges—A geomorphological map from Brúarjökull, East Iceland, *J. Maps*, *4*(1), 5–20, doi:10.4113/jom.2008.91.
Klages, J. P., G. Kuhn, C.-D. Hillenbrand, A. Graham, J. Smith, R. Larter, and K. Gohl (2013), First geomorphological record and glacial history of an inter-ice stream ridge on the West Antarctic continental shelf, *Quat. Sci. Rev.*, *61*, 47–61, doi:10.1016/j.quascirev.2012.11.007.
Knight, P. G. (1987), Observations at the edge of the Greenland ice sheet: Boundary condition implications for modellers, *Int. Assoc. Hydrol. Sci. Publ.*, *170*, 359–366.
Knight, P. G. (1989), Stacking of basal debris layers without bulk freezing-on: Isotopic evidence from West Greenland, *J. Glaciol.*, *35*(120), 214–216.
Knight, P. G. (1997), The basal ice layer of glaciers and ice sheets, *Quat. Sci. Rev.*, *16*, 975–993, doi:10.1016/S0277-3791(97)00033-4.
Kristensen, L., and D. I. Benn (2012), A surge of the glaciers Skobreen-Paulabreen, Svalbard, observed by time-lapse photographs and remote sensing data, *Polar Res.*, *31* 11106, doi:10.3402/polar.v31i0.11106.
Kristensen, L., H. Juliussen, H. H. Christiansen, and O. Humlum (2009), Structure and composition of a tidewater glacier push moraine, Svalbard, revealed by DC resistivity profiling, *Boreas*, *38*, 176–186, doi:10.1111/j.1502-3885.2008.00045.x.
Larsen, N. K., J. A. Piotrowski, P. Christoffersen, and J. Menzies (2006), Formation and deformation of basal till during a glacier surge; Elisebreen, Svalbard, *Geomorphology*, *81*, 217–234, doi:10.1016/j.geomorph.2006.04.018.
Larsen, N. K., C. Kronborg, J. C. Yde, and N. T. Knudsen (2010), Debris entrainment by basal freeze-on and thrusting during the 1995–1998 surge of Kuannersuit Glacier on Disko Island, west Greenland, *Earth Surf. Processes Landforms*, *35*(5), 561–574, doi:10.1002/esp.1945.
Lawson, D. E. (1979), Sedimentological analysis of the western terminus region of the Matanuska Glacier, Alaska *CRREL Report 79-9*, U.S. Army Cold Regions Research and Engineering Laboratory, Hanover.
Lawson, D. E., J. C. Strasser, E. B. Evenson, R. B. Alley, G. J. Larson, and S. A. Arcone (1998), Glaciohydraulic supercooling: A freeze-on mechanism to create stratified, debris-rich basal ice: I. Field evidence, *J. Glaciol.*, *44*(148), 547–562.
Lliboutry, L. (1993), Internal melting and ice accretion at the bottom of temperate glaciers, *J. Glaciol.*, *39*(131), 50–64.
Lønne, I. (2006), Low-velocity glacial surges—Processes unlocked by modern surge on Svalbard, *Geology*, *34*(7), 553–556, doi:10.1130/G21799.1.
Lovell, H., C. R. Stokes, M. J. Bentley, and D. I. Benn (2012), Evidence for rapid ice flow and proglacial lake evolution around the central Strait of Magellan region, southernmost Patagonia, *J. Quat. Sci.*, *27*(6), 625–638, doi:10.1002/jqs.2555.
Lovell, H., E. J. Fleming, D. I. Benn, B. Hubbard, S. Lukas, and K. Naegeli (2015), Evidence for former dynamic flow of a currently cold-based valley glacier on Svalbard revealed by basal ice and structural glaciology investigations, *J. Glaciol.*, *61*(226), 309–328, doi:10.3189/2015JoG14J120.
Lukas, S., et al. (2013), Clast shape analysis and clast transport paths in glacial environments: A critical review of methods and the role of lithology, *Earth Sci. Rev.*, *121*, 96–116, doi:10.1016/j.earscirev.2013.02.005.
Moore, P. L., N. R. Iverson, and D. Cohen (2010), Conditions for thrust faulting in a glacier, *J. Geophys. Res.*, *115*, F02005, doi:10.1029/2009JF001307.
Murray, T., D. L. Gooch, and G. W. Stuart (1997), Structures within the surge front at Bakaninbreen using ground penetrating radar, *Ann. Glaciol.*, *24*, 122–129.

Nye, J. (1970), Glacier sliding without cavitation in a linear viscous approximation, *Proc. R. Soc. London A. Math. Phys. Sci.*, *315*(1522), 381–403, doi:10.1098/rspa.1970.0050.

Ó Cofaigh, C., and D. J. A. Evans (2001), Deforming bed conditions associated with a major ice stream of the last British ice sheet, *Geology*, *29*(9), 795–798, doi:10.1130/00917613(2001)029<0795:DBCAWA>2.0.CO;2.

Ottesen, D., and J. A. Dowdeswell (2006), Assemblages of submarine landforms produced by tidewater glaciers in Svalbard, *J. Geophys. Res.*, *111*, F01016, doi:10.1029/2005JF000330.

Ottesen, D., J. A. Dowdeswell, D. I. Benn, L. Kristensen, H. H. Christiansen, O. Christensen, L. Hansen, E. Lebesbye, M. Forwick, and T. O. Vorren (2008), Submarine landforms characteristic of glacier surges in two Spitsbergen fjords, *Quat. Sci. Rev.*, *27*, 1583–1599, doi:10.1016/j.quascirev.2008.05.007.

Rea, B. R., and D. J. A. Evans (2011), An assessment of surge-induced crevassing and the formation of crevasse squeeze ridges, *J. Geophys. Res.*, *116*, F04005, doi:10.1016/j.quascirev.2008.05.007.

Roberts, D. H., and J. K. Hart (2005), The deforming bed characteristics of a stratified till assemblage in north East Anglia, UK: Investigating controls on sediment rheology and strain signatures, *Quat. Sci. Rev.*, *24*(1), 123–140, doi:10.1016/j.quascirev.2004.03.004.

Roberts, D. H., J. C. Yde, N. T. Knudsen, A. J. Long, and J. M. Lloyd (2009), Ice marginal dynamics during surge activity, Kuannersuit Glacier, Disko Island, West Greenland, *Quat. Sci. Rev.*, *28*, 209–222, doi:10.1016/j.quascirev.2008.10.022.

Sharp, M. (1985), "Crevasse-fill" ridges—A landform type characteristic of surging glaciers?, *Geogr. Ann.*, *67A*(3-4), 213–220.

Sharp, M., J. Jouzel, B. Hubbard, and W. Lawson (1994), The character, structure and origin of the basal ice layer of a surge-type glacier, *J. Glaciol.*, *40*(135), 327–340.

Solheim, A., and S. L. Pfirman (1985), Sea-floor morphology outside a grounded, surging glacier; Bråsvellbreen, Svalbard, *Mar. Geol.*, *65*, 127–143, doi:10.1016/0025-3227(85)90050-7.

Souchez, R., and J. Jouzel (1984), On the isotopic composition in δD and $\delta^{18}O$ of water and ice during freezing, *J. Glaciol.*, *30*(106), 369–372.

Souchez, R., R. Lorrain, and J. L. Tison (1988), Co-isotopic signature of two mechanisms of basal-ice formation in Arctic outlet glaciers, *Ann. Glaciol.*, *10*, 163–166.

Sugden, D., C. M. Clapperton, J. Gemmell, and P. Knight (1987), Stable isotopes and debris in basal glacier ice, South Georgia, Southern Ocean, *J. Glaciol.*, *33*(115), 324–329.

Swift, D. A., D. J. A. Evans, and A. E. Fallick (2006), Transverse englacial debris-rich ice bands at Kviárjökull, southeast Iceland, *Quat. Sci. Rev.*, *25*, 1708–1718, doi:10.1016/j.quascirev.2006.01.003.

Waller, R. (1997), The role of tectonism in the distribution, appearance and dynamic behaviour of debris-rich basal ice, PhD thesis, School of Physical and Geographical Sciences, Keele University, Keele, Staffordshire, U. K.

Waller, R., J. Hart, and P. Knight (2000), The influence of tectonic deformation on facies variability in stratified debris-rich basal ice, *Quat. Sci. Rev.*, *19*, 775–786, doi:10.1016/S0277-3791(99)00035-9.

Weertman, J. (1961), Mechanism for the formation of inner moraines found near the edge of cold ice caps and ice sheets, *J. Glaciol.*, *3*(30), 965–978.

Woodward, J. T., T. Murray, and A. McCaig (2002), Formation and reorientation of structure in the surge-type glacier Kongsvegen, Svalbard, *J. Quat. Sci.*, *17*(3), 201–209, doi:10.1002/jqs.673.

Yde, J. C., N. T. Knudsen, N. K. Larsen, C. Kronborg, O. B. Nielsen, J. Heinemeier, and J. Olsen (2005), The presence of thrust-block naled after a major surge event: Kuannersuit Glacier, West Greenland, *Ann. Glaciol.*, *42*(1), 145–150, doi:10.1016/j.jhydrol.2004.06.008.